



21st Century Tools for Nanotoxicology: Transcriptomic Biomarker Panel and Precision-Cut Lung Slice Organ Mimic System for the Assessment of Nanomaterial-Induced Lung Fibrosis

Rahman, Luna; Williams, Andrew; Gelda, Krishna; Nikota, Jake; Wu, Dongmei; Vogel, Ulla Birgitte; Halappanavar, Sabina

Published in:
Small

Link to article, DOI:
[10.1002/sml.202000272](https://doi.org/10.1002/sml.202000272)

Publication date:
2020

Document Version
Publisher's PDF, also known as Version of record

[Link back to DTU Orbit](#)

Citation (APA):

Rahman, L., Williams, A., Gelda, K., Nikota, J., Wu, D., Vogel, U. B., & Halappanavar, S. (2020). 21st Century Tools for Nanotoxicology: Transcriptomic Biomarker Panel and Precision-Cut Lung Slice Organ Mimic System for the Assessment of Nanomaterial-Induced Lung Fibrosis. *Small*, 16, Article e2000272. <https://doi.org/10.1002/sml.202000272>

General rights

Copyright and moral rights for the publications made accessible in the public portal are retained by the authors and/or other copyright owners and it is a condition of accessing publications that users recognise and abide by the legal requirements associated with these rights.

- Users may download and print one copy of any publication from the public portal for the purpose of private study or research.
- You may not further distribute the material or use it for any profit-making activity or commercial gain
- You may freely distribute the URL identifying the publication in the public portal

If you believe that this document breaches copyright please contact us providing details, and we will remove access to the work immediately and investigate your claim.

21st Century Tools for Nanotoxicology: Transcriptomic Biomarker Panel and Precision-Cut Lung Slice Organ Mimic System for the Assessment of Nanomaterial-Induced Lung Fibrosis

Luna Rahman, Andrew Williams, Krishna Gelda, Jake Nikota, Dongmei Wu, Ulla Vogel, and Sabina Halappanavar*

There is an urgent need for reliable toxicity assays to support the human health risk assessment of an ever increasing number of engineered nanomaterials (ENMs). Animal testing is not a suitable option for ENMs. Sensitive *in vitro* models and mechanism-based targeted *in vitro* assays that enable accurate prediction of *in vivo* responses are not yet available. In this proof-of-principle study, publicly available mouse lung transcriptomics data from studies investigating xenobiotic-induced lung diseases are used and a 17-gene biomarker panel (PFS17) applicable to the assessment of lung fibrosis is developed. The PFS17 is validated using a limited number of *in vivo* mouse lung transcriptomics datasets from studies investigating ENM-induced responses. In addition, an *ex vivo* precision-cut lung slice (PCLS) model is optimized for screening of potentially inflammogenic and pro-fibrotic ENMs. Using bleomycin and a multiwalled carbon nanotube, the practical application of the PCLS method as a sensitive alternative to whole animal tests to screen ENMs that may potentially induce inhalation toxicity is shown. Conditional to further optimization and validation, it is established that a combination of PFS17 and the *ex vivo* PCLS method will serve as a robust and sensitive approach to assess lung inflammation and fibrosis induced by ENMs.

1. Introduction

Engineered nanomaterials (ENMs, materials in the size scale of 1–100 nm) are application-tailored, sophisticated materials that exhibit functionally diverse physical, chemical, and biological properties, and as a result, are desirable for various consumer applications. Toxicological research, based mainly on animal testing, has shown that ENMs are potentially harmful to humans when inhaled or consumed.^[1–5]

When conducting research for the purposes of human health risk assessment (HHRA) and in support of regulatory decisions, *in vivo* animal models are the standard. Animal testing enables investigation of the intact biological specimen, but it is animal intensive, as well as cost and time prohibitive. More importantly, it is not a feasible testing option for emerging substances such as ENMs and

their wide range of physicochemical variants. Animal test surrogates are available, including organ/tissue culture and *in vitro* cell culture systems that range from simple monolayer cultures to sophisticated co-cultures involving multiple cell types. Although studies investigating the potential toxic responses to ENMs using *in vitro* systems outnumber the published *in vivo* exposure studies, the biological relevance of data generated using *in vitro* systems remains questionable. In most cases, the results of *in vitro* tests indicate toxicity (measured mainly by cytotoxicity assays); however, in subsequent applications such as risk assessment, the data are often considered irrelevant as they do not describe the *in vivo* response they are intended to predict or are not predictive of a response observed *in vivo* in animals or in humans.


Attempts are made to establish representative *in vitro* systems that reflect healthy and whole organ responses to xenobiotic exposure but not without significant challenges. For example, lung epithelial cells derived from normal or cancerous lung tissue from different species are used to assess substance-induced lung toxicity. However, the lung is a multicellular organ and simple monocultures or even complex cultures involving

Dr. L. Rahman, A. Williams, K. Gelda, Dr. J. Nikota, D. Wu, Dr. S. Halappanavar
Environmental Health Science and Research Bureau
Health Canada

Sir Frederick G Banting Research Centre
251 Sir Frederick Banting Driveway, Building 22
Ottawa, ON K1A 0K9, Canada
E-mail: sabina.halappanavar@canada.ca

Prof. U. Vogel
National Research Centre for the Working Environment
Lersø Parkallé 105, Copenhagen 2100, Denmark

Prof. U. Vogel
Department of Micro- and Nanotechnology
Technical University of Denmark
Building 101A 2800 Copenhagen, Lyngby, Denmark

 The ORCID identification number(s) for the author(s) of this article can be found under <https://doi.org/10.1002/sml.202000272>.

© 2020 Her Majesty the Queen in Right of Canada. Published by Wiley-VCH Verlag GmbH & Co. KGaA. Reproduced with the permission of the Minister of Health Canada. This is an open access article under the terms of the Creative Commons Attribution License, which permits use, distribution and reproduction in any medium, provided the original work is properly cited.

The copyright line for this article was changed on 22 June 2020 after original online publication.

DOI: 10.1002/sml.202000272

multiple lung cell types do not capture the co-ordinated responses of different cell types in the lungs. In addition to the simplicity of the *in vitro* systems, the *in vitro* assays, endpoints, and specific biomarkers chosen for measuring responses are not mechanism-informed and are often limited to the experiences and expertise of the respective investigator. In the context of ENMs, additional constraints, such as lack of clear understanding of the *in vivo* mechanisms of toxicity,^[6] have made it difficult to design the appropriate *in vitro* assays targeting *in vivo* response. As a result, after almost two decades of intense toxicological research, quality quantitative data for HHRA is not available for most ENMs and an acceptable HHRA framework has yet to be developed.

In recent years, there has been increasing interest in the use of omics data to inform the design and development of *in vitro* biomarkers that are predictive of *in vivo* toxicity. Toxicogenomics investigates global responses induced following chemical exposure at the level of the genome, transcriptome, proteome, and metabolome. Of these, genome-wide mRNA expression analysis or transcriptomics technologies are extensively used and readily applied in toxicology for identifying the underlying mechanisms of substance-induced toxicity. Transcriptomic perturbations that occur very early following exposure to a substance of interest can be related to apical toxicity endpoints measured in both *in vivo* and *in vitro* experiments and are characteristic of the adverse outcomes observed in intact organisms. Transcriptomics tools have been successfully used as an alternative approach to comprehensively investigate the toxicological response induced by various classes of ENMs and to identify the properties of ENMs that are responsible for eliciting adverse effects.^[7–14] However, in order for toxicogenomics data to be effectively applied in safety assessment or predictive toxicology, it is essential to identify and discriminate genes that define tissue defense mechanisms from those potentially critical for the progression of toxic outcomes and diseases.

We previously used a meta-analysis approach to query publicly available transcriptomic datasets describing specific lung diseases and ENMs-induced responses, to identify gene features,^[15] and functionally related bi-clusters of genes that are associated with lung pathology following ENMs exposure.^[16,17] These approaches identified the essential transcriptional signatures of diseases that can be measured early after exposure and provided insight into the underlying mechanisms of ENMs-induced toxicities. The mechanistic information gathered was further used to identify toxicity pathways involved in ENMs-induced lung pathologies and an adverse outcome pathway (AOP) for ENMs-induced lung fibrosis. This AOP clearly identifies the key events in the progression of lung fibrosis (the detailed AOP can be found at <https://aopwiki.org/aops/173>).^[9,18]

In the present study, we developed a 17-gene pro-fibrotic biomarker panel (here after referred to as PFS17) that is specifically predictive of lung fibrosis in mice. Previously published, publicly available gene expression microarray data from mouse lungs exposed to a variety of stressors that are known to cause lung disease (i.e., lung inflammation, emphysema, chronic obstructive pulmonary disease [COPD], lung fibrosis, and lung cancer) were used.^[19–30] The PFS17 was pre-validated using transcriptomics data generated in-house from mice exposed to multi-walled carbon nanotubes (MWCNTs) that are suspected

to induce fibrosis in mouse lungs. Furthermore, an *ex vivo* precision-cut lung slice (PCLS) technique, an alternative to whole animal testing, was optimized for the assessment of lung fibrosis using bleomycin as a model pro-fibrotic agent and was tested for its applicability to assess ENMs-induced lung fibrosis for the HHRA purpose.

2. Results

The training set consisted of lung gene expression profiles derived from 12 individual publicly available transcriptomic datasets that describe characteristic features of lung diseases (Table 1 and Table S1, Supporting Information). From this, PFS17 (a panel of 17 pro-fibrotic genes; Table 2) was identified to classify substances as pro-fibrotic (PF) or non-fibrotic (NF). Figure 1 shows the principal component analysis (PCA) performed using the *prcomp* function in R using the training dataset. The scatter plot of the first two principal components is presented. The red line reflecting the first principal component clearly shows the contrast between the PF and NF classes highlighting a distinct separation between the two classes with the exception of two studies involving bacterial infection and tumor. Bacterial infection can trigger pro-fibrotic reactions,^[31] and tumor formation is shown to be associated with fibrotic lesions.^[32] The grey line separates ten profiles that are borderline PF with their first principal component being negative. Many of these profiles were classified as unknown from the shrunken centroid analysis. Figure 2 shows the heatmap of the PFS17. With the exception of two studies, all studies that were assigned to the PF class were correctly predicted as PF. In accordance with the results shown in Figure 1, among the studies assigned to an NF class, many of them were classified as unknown.

2.1. Validation of PFS17 Using Publicly Available Transcriptomics Studies

The PFS17 was validated using a limited number of publicly available *in vivo* lung transcriptomics datasets. The PCA loadings obtained from the analysis of training set data was applied to the transcriptomic profiles obtained from studies involving the PF stressors bleomycin, ozone, radiation, and MWCNTs. The PCA plots and heat maps (Figures S1–S38, Supporting Information) show the data from the training set in red (PF) and blue (NF) circles, with each individual validation study displayed as a green triangle with labels in green font. Separate PCA plots and heatmaps are presented for each study grouped by the stressors. Table S2, Supporting Information, lists all datasets included in the validation set and the class prediction results.^[9,12,14,33–44] Figures 3 and 4 show heatmaps of all non-nano and nano studies included in the validation dataset. The validation set consisted of three bleomycin studies with 12 individual experimental conditions reflecting different exposure concentrations and post-exposure time points. With the exception of two experimental conditions from a single study, all studies involving bleomycin were classified as PF or borderline PF (Figures S1–S6, Supporting Information). Similarly, 16 experimental conditions from three individual studies investigating ozone-induced lung

Table 1. Studies used in the development of the PFS17 gene signature.

Phase	GEO accession no.	Ref.	Gene expression platform	Strain	Disease model
Training set	GSE4231	[19]	UCSF 10Mm Mouse v.2 Oligo Array (GPL1089); UCSF GS Operon Mouse v.2 Oligo Array (GPL3330); UCSF 11Mm Mouse v.2 Oligo Array (GPL3331); UCSF 7Mm Mouse v.2 Oligo Array (GPL3359)	C57BL/6; BALB/c; C3H; transgenic mice expressing IL-13 under the control of a Clara cell-specific promoter	Lung inflammation models
	GSE6116	[20]	Affymetrix Mouse Genome 430 2.0 Array (GPL1261)	5-week-old female B6C3F1	Biomarkers to predict female mouse lung tumors
	GSE6858	[21]	Affymetrix Mouse Genome 430 2.0 Array (GPL1261)	8-week-old BALB/c and BALB-RAG	Model of experimental asthma
	GSE8790	[22]	Affymetrix Mouse Genome 430 2.0 Array (GPL1261)	A/J mouse strain (Jackson Lab)	Cigarette smoke-induced emphysema
	GSE11037	[23]	Agilent-011978 Mouse Microarray G4121A (GPL891)	C57BL/6; SP-C/TNF- α	Emphysema
	GSE18534	[24]	Affymetrix Mouse Genome 430 2.0 Array (GPL1261)	RB-p53 double knockout mouse; RB-p53-p130 triple knockout mouse	Mouse small cell lung cancer model
	GSE19605	[25]	Illumina MouseRef-8 v2.0 expression beadchip (GPL6885)	Wildtype or CC-LR (a Clara cell-targeted K-ras mutant mouse model of lung cancer)	Lung carcinogenesis
	GSE25640	[26]	Affymetrix Mouse Genome 430 2.0 Array (GPL1261)	C57BL/6 and C57BL/6 with FIZZ2 knockout	Pulmonary fibrosis
	GSE31013	[27]	Affymetrix Mouse Genome 430 2.0 Array (GPL1261)	B6C3F1	Spontaneous lung tumors
	GSE40151	[28]	Affymetrix Mouse Genome 430 2.0 Array (GPL1261)	C57BL6/J	Idiopathic pulmonary fibrosis
	GSE42233	[29]	Illumina Mouse WG-6 v2.0 expression beadchip (GPL6887)	129S2 K-rasLA1	Lung cancer
	GSE52509	[30]	Illumina MouseRef-8 v2.0 expression beadchip (GPL6885)	C57BL/6N	Chronic obstructive pulmonary disease (COPD)

fibrotic responses were included in the validation set, of which only two experimental conditions were classified as borderline PF with all others classified as NF (Figures S7–S12, Supporting Information). Of the four separate radiation studies, only 1 of the 27 experimental conditions were classified as borderline PF (Figures S13–S20, Supporting Information). While PFS17 was best at predicting bleomycin-induced lung fibrosis, it was not effective in classifying the ozone or radiation-induced fibrotic response. Pertinent to ENMs, a total of six individual studies investigating MWCNT-induced lung responses were included in the validation set that consisted of 82 different exposure concentrations and post-exposure time points. Application of PFS17 to MWCNT datasets revealed 22, 26, and 34 experimental conditions were classified as PF, borderline PF, or NF, respectively (Figures S21–S38, Supporting Information). Half of all MWCNT datasets were classified as borderline PF or PF; the classification did not follow any particular dose, post-exposure time, or MWCNT-specific trend, although high dose studies were more likely to be binned as PF or borderline PF.

2.2. Optimization of PCLS Culture Conditions

2.2.1. Impact of Slice Thickness, Incubation Conditions, and Culture Time on PCLS Viability

Before using the PCLS for testing ENMs-induced lung responses, the impact of slice thickness and culturing

conditions (stagnant versus moving/rocking conditions) on slice health and slice viability over the intended duration of culture was assessed using the lactate dehydrogenase (LDH) cytotoxicity assay. The PCLS of 250 or 500 μ m thickness were cultured in PCLS medium at 37 °C. The LDH release was assessed at different time points (Figure 5A). Comparison of viability of 250 versus 500 μ m slice thickness showed that 250 μ m PCLS remained healthy on day 1 and by day 3, began to show signs of toxicity, which was increased by day 7 in culture. The 500 μ m slices showed no signs of toxicity for up to 7 days (Figure 5A) in culture, which was also confirmed by the histological analysis of haematoxylin and eosin (H&E) stained slices (Figure 5B). In addition, culturing PCLS in stagnant or rocking conditions did not impact slice health. Based on these results, all experiments investigating acute endpoints were conducted using 250 μ m thick slices. For the long-term experiments including histopathology requiring more than 2 days of culture, 500 μ m slices were used. Slices were cultured throughout experiments without rocking under stagnant conditions.

2.2.2. Selection of MWCNT Dose

Dose Selection, Viability, and Interaction of Mitsui-7 with Cells in PCLS Following Exposure: Since the PCLS technique was being optimized for its application in the assessment of ENMs-induced lung responses and pathology, all optimizing experiments were conducted mainly using Mitsui-7 MWCNT, which

Table 2. Genes in the PFS17 biomarker set.

Gene symbol	Accession no.	Gene name
<i>Arg1</i>	NM_007482.3	Mus musculus arginase 1, liver (<i>Arg1</i>), mRNA
<i>C1qb</i>	NM_009777.2	Mus musculus complement component 1, q subcomponent, beta polypeptide (<i>C1qb</i>), mRNA
<i>Ccl9</i>	NM_011338.2	Mus musculus chemokine (C-C motif) ligand 9 (<i>Ccl9</i>), mRNA
<i>Ccr5</i>	NM_009917.5	Mus musculus chemokine (C-C motif) receptor 5 (<i>Ccr5</i>), mRNA
<i>Ch25h</i>	NM_009890.1	Mus musculus cholesterol 25-hydroxylase (<i>Ch25h</i>), mRNA
<i>Clec4a2</i>	NM_001170333.1	Mus musculus C-type lectin domain family 4, member a2 (<i>Clec4a2</i>), transcript variant 1, mRNA
<i>Ctss</i>	NM_021281.3	Mus musculus cathepsin S (<i>Ctss</i>), transcript variant 2, mRNA
<i>Fcgr2b</i>	NM_001077189.1	Mus musculus Fc receptor, IgG, low affinity IIb (<i>Fcgr2b</i>), transcript variant 1, mRNA
<i>Fxyd4</i>	NM_001173372.1	Mus musculus FXYD domain-containing ion transport regulator 4 (<i>Fxyd4</i>), transcript variant 2, mRNA
<i>Itgb2</i>	NM_008404.4	Mus musculus integrin beta 2 (<i>Itgb2</i>), mRNA
<i>Lpxn</i>	NM_134152.3	Mus musculus leupaxin (<i>Lpxn</i>), mRNA
<i>Ly86</i>	NM_010745.2	Mus musculus lymphocyte antigen 86 (<i>Ly86</i>), mRNA
<i>Retnla</i>	NM_020509.3	Mus musculus resistin like alpha (<i>Retnla</i>), mRNA
<i>S100a4</i>	NM_011311.2	Mus musculus S100 calcium binding protein A4 (<i>S100a4</i>), mRNA
<i>Serpina3g</i>	NM_009251.2	Mus musculus serine (or cysteine) peptidase inhibitor, clade A, member 3G (<i>Serpina3g</i>), transcript variant 1, mRNA
<i>Serpina3n</i>	NM_009252.2	Mus musculus serine (or cysteine) peptidase inhibitor, clade A, member 3N (<i>Serpina3n</i>), mRNA
<i>Slc26a4</i>	NM_011867.4	Mus musculus solute carrier family 26, member 4 (<i>Slc26a4</i>), mRNA

has been shown to induce lung fibrosis in previous studies.^[45–47] A dose-range study was conducted using 250 or 500 μm PCLS exposed to different concentrations of Mitsui-7. Any concentration above 100 $\mu\text{g mL}^{-1}$ was cytotoxic (data not shown) and thus, for the remaining experiments, concentrations of 100 $\mu\text{g mL}^{-1}$ and below were used. The LDH assay results showed no cytotoxicity on day 1 post-exposure of 250 μm slices or up to 7 days after exposure of 500 μm slices to any tested doses of Mitsui-7, compared to the matched vehicle only treated controls (Figure 5C,D). Since exposures to ENMs resulted in subtle or no cytotoxicity, the above-mentioned concentrations were used in the subsequent experiments.

Based on Kunst et al. 2009,^[48] the average alveolar surface area (which accounts for most of the surface area in lungs) in C57BL/6 mice is 82.2 cm^2 and the left lung comprises 32% of

that total alveolar surface area. This means that the alveolar surface area of the left mouse lung is estimated to be 26.304 cm^2 . The total number of slices we could theoretically harvest from a left mouse lobe is 12 (500 μm thickness) and 24 (250 μm thickness) slices (in the present study, left lung was sectioned to obtain ≈ 9 (500 μm thickness) and ≈ 18 (250 μm thickness) undamaged slices of uniform thickness, which represents $\approx 75\%$ of the left lung tissue). By this calculation method, surface area for each slice is estimated to be 2.191 $\text{cm}^2/500 \mu\text{m}$ slice and 1.096 $\text{cm}^2/250 \mu\text{m}$ slice (the total alveolar surface area of the left lobe divided by theoretical number of slices). Thus, the 100 $\mu\text{g mL}^{-1}$ MWCNT exposure dose in 0.5 mL volume is equivalent to 45.62 and 22.82 $\mu\text{g cm}^2$ in 250 and 500 μm slices, respectively. For a 50 $\mu\text{g mL}^{-1}$ MWCNT exposure, the dose would be equivalent to 22.81 and 11.41 $\mu\text{g cm}^2$ in 250 and 500 μm , slices, respectively. These doses are comparable to in vitro doses used in Poulsen et al. 2013,^[12] but are high with relation to in vivo intratracheal instillation doses used in the same study.

Notable amounts of Mitsui-7 were present in PCLS 12 h post-exposure and Mitsui-7 fibers were seen evidently penetrating the slices (Figure 6A). Hyperspectral mapping of H&E stained images of PCLS exposed to media control or Mitsui-7 was conducted to determine if MWCNTs interact with PCLS ex vivo in a similar way to what is observed in vivo. In our previous studies, we have successfully applied hyperspectral mapping to localize ENMs in lung tissue from mice.^[9,14] As each pixel in a hyperspectral image contains spectral information of that spatial pixel area, comparison between the spectral profiles of hyperspectral images of Mitsui-7 in PCLS with the reference spectral libraries created for Mitsui-7 allowed localization and identification of Mitsui-7 in PCLS. The dark field images and corresponding mapped hyperspectral images of PCLS exposed to Mitsui-7 and overlay image are represented in Figure 6B. The areas of the hyperspectral images that matched to reference spectral libraries of Mitsui-7 in PCLS are colored in red and indicated by red arrow heads.

2.3. Applicability of PCLS to Assess ENM-Induced Fibrosis

Upon inhalation or deposition in the lungs, most ENMs induce pulmonary inflammation in vivo. Inflammation is one of the early essential key events identified in the AOP for substance-induced lung fibrosis (AOP173, <https://aopwiki.org/aops/173>).^[9,18] Thus, the ability of PCLS to activate the pro-inflammatory process following exposure to ENMs was assessed in PCLS stimulated with Mitsui-7 by assessing the differential expression of 23 cytokines via the 23-plex cytokine ELISA kit. The supernatant was used in the present study, as secretory proteins playing important roles in disease progressions are readily accessible in cell supernatants.^[49–51]

As shown in Figure 7, the expression of a total of ten cytokines (interleukin 1 beta [IL-1 β], interleukin-5 [IL-5], interleukin-6 [IL-6], interleukin-10 [IL-10], p70 subunit of interleukin-12 [IL-12 (p70)], interleukin-17 [IL-17], granulocyte-colony stimulating factor [G-CSF], macrophage inflammatory protein-1 beta [MIP-1 β], RANTES, and tumor necrosis factor [TNF- α]) was found to be altered in at least one Mitsui-7 dose group by

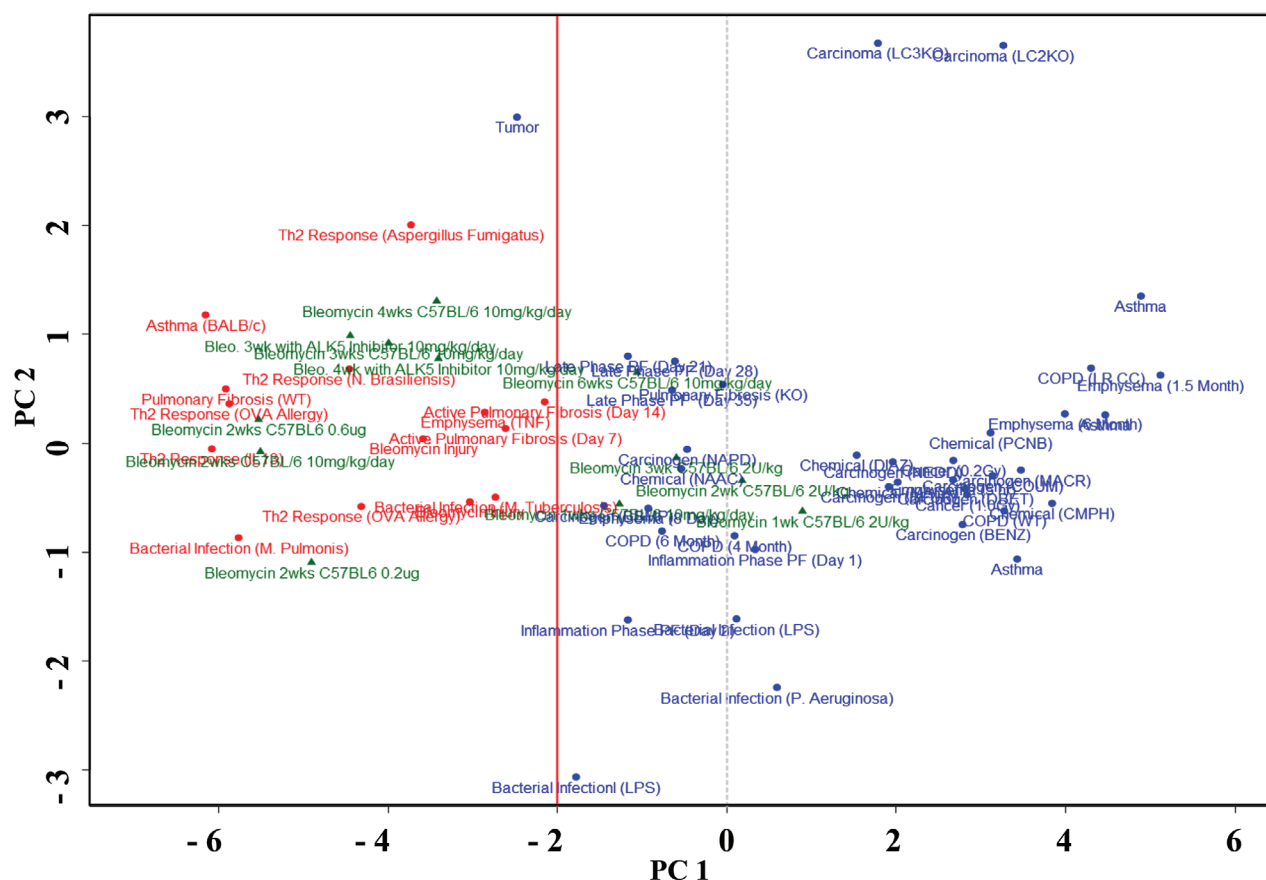
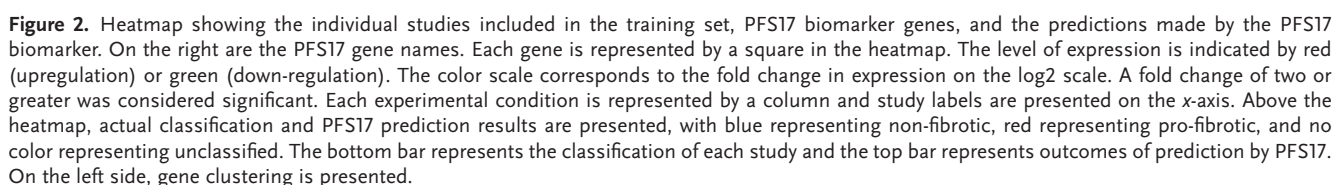


Figure 1. Scatter plot representing the first two components of PCA performed applying the prcomp function in R using the training dataset. The red line reflecting the first principal component clearly shows the contrast between the PF and NF classes highlighting a distinct separation between the two classes with the exception of two studies involving bacterial infection and tumor formation.

≥1.3-fold change compared to the control on day 1 (Figure 7A). The relative expression of cytokines was assessed on day 7 post-exposure to 100 µg mL⁻¹ Mitsui-7 or 100 µg mL⁻¹ bleomycin to assess if inflammation persisted over time. The results did not reveal differential expression of pro-inflammatory mediators in the supernatant, which could be attributed to frequent changes of the medium or degradation of proteins in the supernatant over time. To rule out the possibility of dying PCLS over time following MWCNT exposure, day 7 post-exposure PCLS lysates were assessed by 23-plex ELISA for differential expression of cytokines (Figure 7B). The results showed that expression levels of 16 pro-inflammatory proteins, including interleukin-1 alpha (IL-1α), IL-1β, interleukin-2 (IL-2), interleukin-3 (IL-3), interleukin-9 (IL-9), p40 subunit of interleukin 12 (IL-12 (p40)), IL-17, eotaxin, G-CSF, granulocyte-macrophage colony-stimulating factor (GM-CSF), chemokine (C-X-C motif) ligand-1 (CXCL-1/KC), monocyte chemoattractant protein-1 (MCP-1) or C-C motif chemokine ligand-2 (CCL-2), macrophage inflammatory protein 1 alpha (MIP-1α), MIP-1β, and TNF-α were increased by ≥1.3-fold change compared to the control on day 7 post Mitsui-7 exposure. Bleomycin treatment resulted in increased expression levels of 14 proteins, including IL-3, interleukin 4 (IL-4), IL-9, IL-10, IL-12 (p40), IL-12 (p70), IL-17, eotaxin, G-CSF, CXCL-1, CCL-2, MIP-1α, MIP-1β, and TNF-α by ≥1.3-fold change compared to the matched controls on day 7 post-exposure.

Lung fibrosis is routinely reported in studies investigating the toxicity of ENMs, which is manifested following ENMs inhalation or instillation in rodents. In order to determine if lung fibrosis can be induced ex vivo, the expression levels of classic early pro-fibrotic markers CCL-2, osteopontin (OPN), and transforming growth factor beta (TGF-β) was assessed by ELISA on day 1 post-exposure of PCLS (Figure S40B, Supporting Information). Following stimulation with Mitsui-7, levels of CCL-2 were increased by 3.8-, 3.9-, and 6.3-fold in low, medium, and high doses, respectively, compared to the untreated controls. Similarly, there was a 6.4-, 5.7-, and 9.2-fold increase in the expression of OPN, and 3.1-, 2.4-, and 2.9-fold increase in TGF-β levels compared to the untreated controls in the low, mid, and high dose groups, respectively. The increase was dose-dependent in most cases and was statistically significant at all doses tested. It was interesting to note that treatment of PCLS with lipopolysaccharides (LPS), a pro-inflammatory endotoxin, resulted in increased CCL-2 expression, which is also known to play a role in the process of inflammation, but this treatment did not alter OPN or TGF-β expression. Analysis of CCL-2 and TGF-β at day 5 and day 7 post-exposure to Mitsui-7 and bleomycin revealed a significant increase in the levels of the two markers in PCLS exposed to bleomycin, but not in Mitsui-7-exposed PCLS (Figure S40B, Supporting Information).



The images in **Figure 8** represent the histopathological analyses of PCLS exposed to media control, Mitsui-7, or bleomycin. H&E stained lung slices exposed to media only showed minimal morphological changes with scattered small inflammatory foci on day 5 (Figure 8a) and day 7 (Figure 8j), whereas PCLS exposed to Mitsui-7 (Figure 8b,k) or bleomycin (Figure 8c,l) showed moderate changes including lesions around the junctions of the terminal bronchioles and alveolar ducts on day 5 and day 7. The inflammatory foci in PCLS exposed to Mitsui-7 or bleomycin were larger compared to the control samples. These lesions predominantly consisted of macrophages in controls but included activated neutrophils and lymphocytes in exposed PCLS. Masson trichrome staining of PCLS exposed to Mitsui-7 (Figure 8e) or bleomycin (Figure 8f) showed a mild increase in collagen deposition in the area of localized inflammatory foci compared to the control samples (Figure 8d) on day 5. The

Since the ex vivo PCLS model effectively responded to stimulation by the pro-inflammatory and pro-fibrotic stressors MWCNTs and bleomycin, further experiments were conducted using quantitative real-time PCR (RT-qPCR) array to determine if the observed pro-fibrotic pathology ex vivo corresponds to the altered expression levels of genes included in the PFS17 panel. **Figure 9** shows the differential expression PFS17 genes. On day 1 post-exposure, bleomycin induced upregulation of 11 genes and on day 7 post-exposure, 15 genes showed differential expression with fold changes ≥ 1.5 . On day 1, *Retnla* (4.03), *Serpina3g*

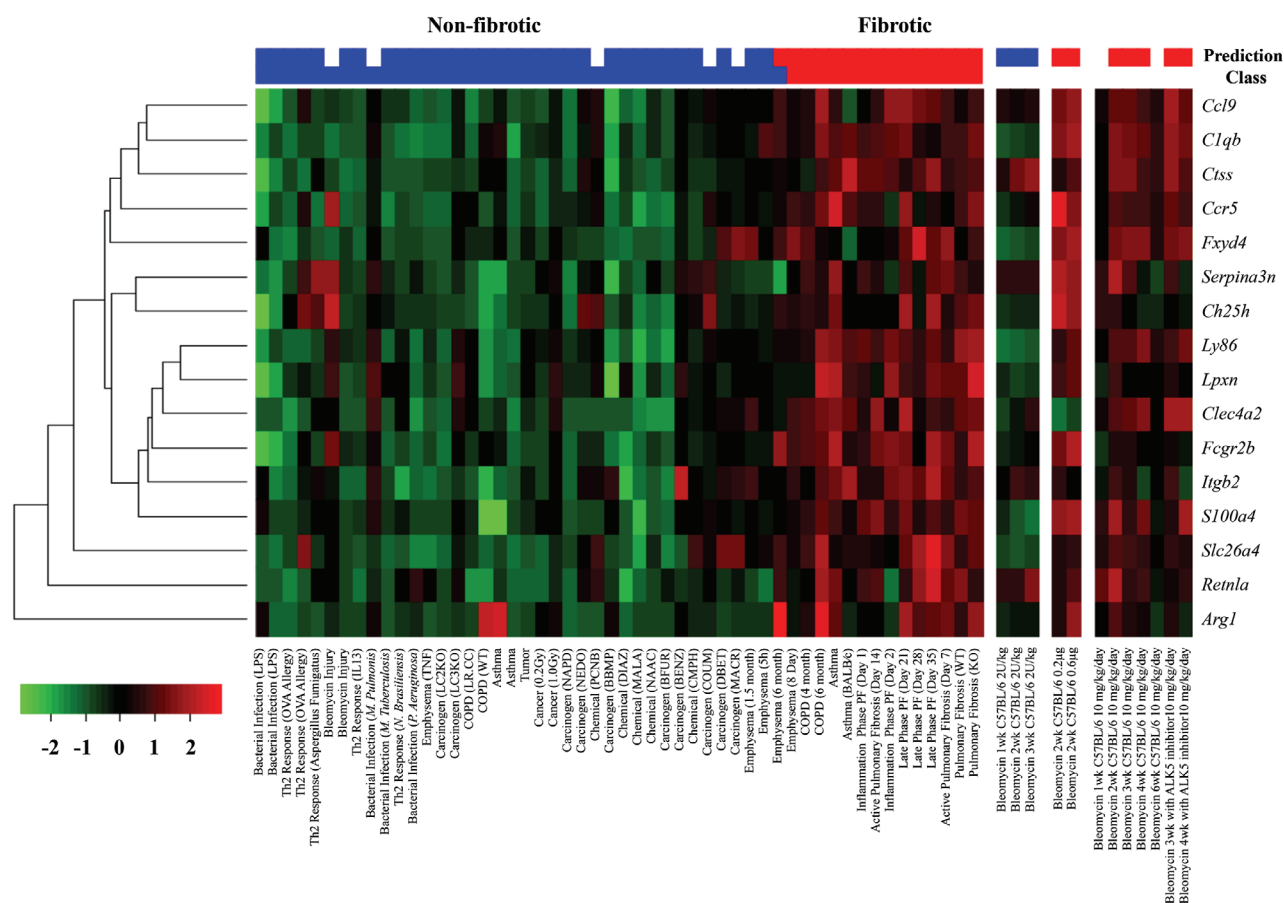


Figure 3. Heatmap showing three bleomycin studies (GEO accession no. GSE8553, GSE34814, GSE132869) included in the validation set, PFS17 genes, and the PFS17 predictions. Gene names are presented on the right. The level of expression (log2 fold change) is indicated by red (upregulation) or green (down-regulation) squares in the plot. A fold change of two or greater was considered significant. Each experimental condition is represented as a column and study labels are on the x-axis. Above the heatmap, classification and prediction results are presented, with blue representing non-fibrotic, red representing pro-fibrotic, and no color representing unclassified. Class represents the classification of each study and prediction represents outcomes of PFS17 classification.

(4.00), *Lpxn* (1.69), *Ch25h* (2.81), and *Arg1* (3.85) were among the most differentially expressed genes. *Retnla* stimulates immunity-related genes, whereas *Lpxn* and *Ch25h* regulates cell adhesion and cholesterol/lipid metabolism. *Arg* is known to be involved in cytoskeletal rearrangement. *Slc26a4* is suggested to play a role in many respiratory diseases though producing pendrin protein, whereas *Serpina3n* is involved in muscle damage. *Retnla* (43.31), *Serpina3n* (36.46), *Serpina3g* (13.03), *Lpxn* (11.56), *Slc26a4* (10.02), and *Ch25h* (8.38) were among the most highly differentially expressed genes on day 7. On the contrary, the responses to Mitsui-7 were not as robust. On day 1 post-exposure, only two genes showed upregulated expression (*Clqb*, 1.75) and *Arg1* (1.56), and six genes showed down-regulated expression: *Serpina3n* (-1.79), *Lpxn* (-1.68), *Slc26a4* (-1.82), *Ch25h* (-1.71), *S100a4* (-1.53), and *Ccl9* (-1.60). On day 5, no PFS17 genes showed differential expression in Mitsui-7 treated PCLS. On day 7 post-exposure, 4 genes (*Retnla*, 4.01), *Serpina3n* (1.72), *Lpxn* (-2.48), and *Ctss* (1.66) showed differential expression. The number of differentially expressed genes were much higher in PCLS exposed to bleomycin compared to Mitsui-7-treated PCLS at all post-exposure time points tested.

3. Discussion

In the context of ENMs exposure, lung fibrosis is one of the routinely observed pathologies in animals and thus is of high interest and relevance to regulatory scientists.^[9,13–15,18,47,52–56] Lung fibrosis is a progressive interstitial lung disease marked by chronic scarring of the lungs. It is a widely investigated occupational hazard and is commonly observed in miners and welders exposed to metal dusts. A wide variety of environmental, pharmacological, and occupational substances and other non-chemical substances, such as microbes and radiation, induce lung fibrosis. Interestingly, regardless of the differences in the types of pro-fibrotic stressors including ENMs and their chemical properties, the underlying mechanisms of substance-induced lung fibrosis seem to share significant similarities, and mostly involve a robust inflammatory response.^[57] As a result, a detailed AOP (AOP173, <https://aopwiki.org/aops/173>), describing the most common pro-fibrotic mechanism and identifying the key measurable events involved in the process, has been recently established, which is applicable to a broad group of substances and ENMs.^[18]

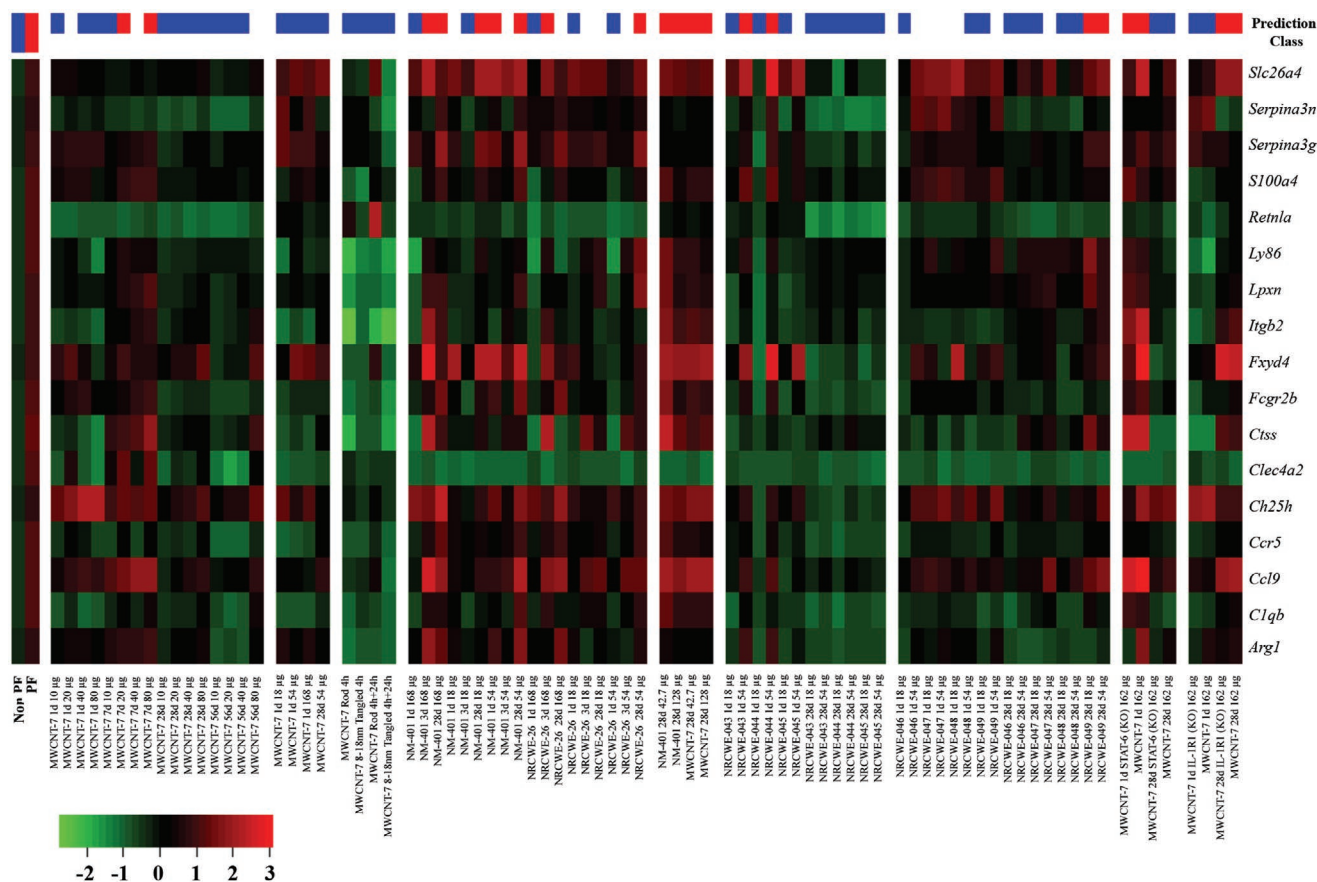


Figure 4. Heatmap showing the individual nano studies included in the validation set, PFS17 biomarker genes, and the PFS17 biomarker classifications. Gene names are indicated on the right. Each gene is represented by a square in the heatmap. The level of expression is indicated by red (upregulation) or green (down-regulation). The color scale corresponds to the fold changes in expression on the log2 scale. A fold change of two or greater was considered significant. On the x-axis, represented by the columns are individual studies. On the far left side, the two columns represent averages of the training dataset classification and prediction outcomes grouped as PF and NF classes. Above the heatmap, classification and prediction results are presented, with blue representing non-fibrotic, red representing pro-fibrotic, and no color representing unknown classification. The bottom bar represents the classification of each study and the top bar represents outcomes of prediction by PFS17.

As stated earlier, animal testing is the preferred approach for testing tissue fibrosis, which is not a preferred option for testing ENMs. With the tremendous advancement of ENMs industry, screening of large numbers of novel ENMs for toxic potential employing a fast and reliable approach becomes necessary. In the present study, an ex vivo lung model that uses fewer animals compared to traditional whole animal testing was optimized to support the effective assessment of the ever growing number of ENMs for their potential to induce lung fibrosis. In addition, using publicly available high content mouse lung transcriptomics data, a 17-gene signature PFS17, which targets assessment of multiple key events identified in the lung fibrosis AOP, was established (AOP173, <https://aopwiki.org/aops/173>).^[9,18] The results showed that the PCLS system can be used to effectively screen ENMs and other substances for lung inflammation and lung fibrosis. The results also determined that PFS17 is a sensitive biomarker panel that can be used to classify pro-fibrotic substances; however, further optimization of PCLS technique and ENMs exposure protocols is required to determine the applicability of PFS17 for the assessment of pro-fibrotic ENMs.

Transcriptional signatures (biomarker genes) that predict toxicity or pathology can facilitate timely and accurate screening of diverse ENMs. The PFS17 was derived from analyzing a wide variety of lung disease models, including bleomycin injury, bacterial infection, lung cancer, and COPD, which seem to exhibit some association with inflammatory and immune responses. The genes included in PFS17 span multiple KEs in the AOP173 from early inflammatory response to late involvement of the fibroblasts in the disease process (<https://aopwiki.org/aops/173>).^[9,18] For example, complement gene *C1qb* and *Fcgr2b* receptor play an important role in the innate immune response and regulation of inflammation,^[58–60] whereas, *S100a4*, *Serpina3g*, and *Serpina3n* are acute phase response genes. Altered expression of CC chemokines (e.g., *Ccl9*) and associated receptors (e.g., *Ccr5*) regulate Th2 response signaling and have been strongly associated with the process of lung fibrosis. The down-regulated expression of *Ccr5* has been observed in idiopathic pulmonary fibrosis.^[61] *Arg1* is induced by the alveolar macrophages in Th2-driven inflammatory conditions and its upregulated expression is observed in asthma, parasitic infections, and pro-fibrotic disease conditions,^[9,62] and

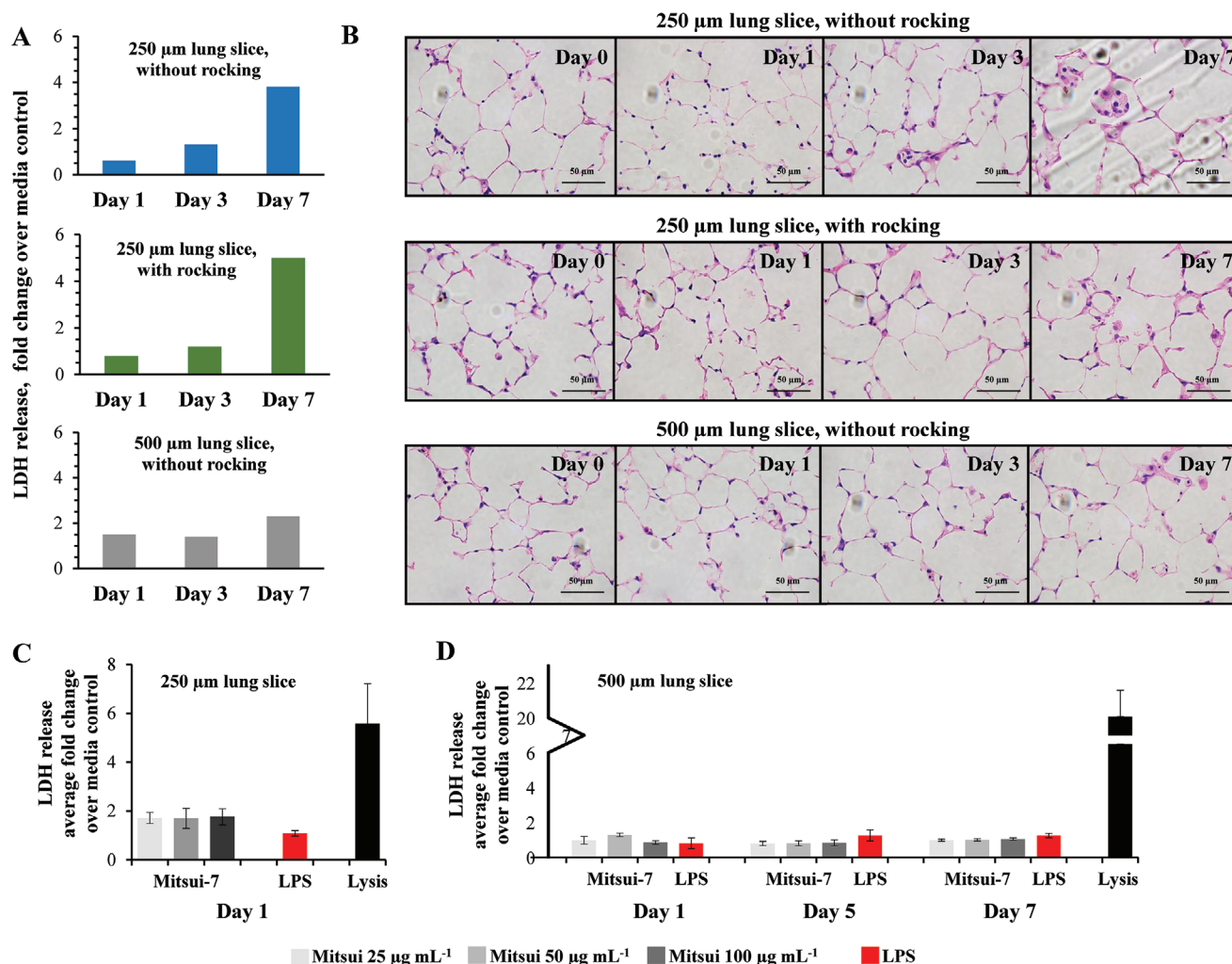


Figure 5. Optimization of PCLS method: A) Influence of slice thickness and culture conditions on slice viability was assessed by the LDH assay (one biological replicate). The results were expressed as fold-change of LDH release compared to the vehicle-treated controls; B) histology images showing PCLS morphology over time; C) 250 μm PCLS viability following exposure to different doses of Mitsui-7 (three biological replicates); D) 500 μm PCLS viability following exposure to different doses of Mitsui-7. The results were expressed as average fold-change of LDH release compared to the vehicle-treated controls (three biological replicates). Lysis buffer was used as an assay control and LPS was used as an experimental control. * represents statistical significance. Statistical significance was calculated (three biological replicates) using Student's *t*-test ($p \leq 0.1$ and fold change ≥ 1.5). No significant difference was observed in the Mitsui-7 or LPS-treated samples.

in lung fibrosis induced by MWCNTs. *Retnla* is hypothesized to promote wound healing and fibrosis in a Th2-driven inflammatory conditions.^[63] The expression of *Ch25h* was recently shown to be induced in primary lung fibroblasts by the activated eosinophils and was suggested to contribute to the development of IPF.^[64] Thus, the panel of 17 genes included in PFS17 reflect the complex biology perturbed during the process of lung fibrosis and reflect the involvement of multiple cell types and as a result, can be effective for screening pro-fibrotic stressors in ex vivo lung organ surrogate systems.

The underlying mechanisms of lung fibrosis share significant similarities in key events. However, a third of all studies included in the validation set were classified as NF by the PFS17 biomarker. A detailed analysis of the experimental designs applied in the studies above did not clarify why some studies expected to be classified as PF were classified as NF. It is

important to note that PFS17 is derived from a training dataset that included a variety of studies and diverse microarray platforms. The heterogeneity and variables present in the training data set resulted in a limited gene space of 9000 genes found at the intersection of all these studies for use in the development of PFS17. However, the validation dataset consisted of studies derived from only two microarray platforms and most of them were derived from similar experimental conditions, which considerably reduced the variability and resulted in expanded gene space of 20000 genes.^[65] Lack of concordance in gene space covered suggests that not all biology perturbed may have been captured by PFS17. It is known that many genes and pathways involved in early inflammation and immune response exhibit redundancy and pleiotropy, which may not be effectively represented in PFS17 due to the small subset of genes used in establishing it. Moreover, fibrosis is a progressive disease that solely

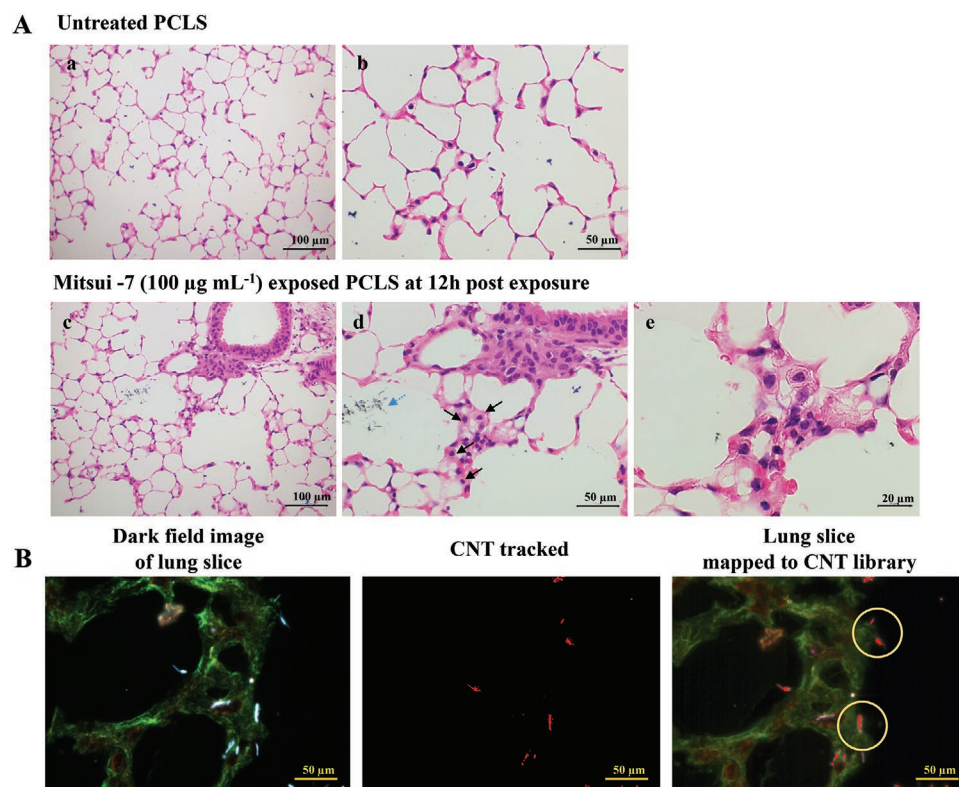


Figure 6. A) Optical light microscopy of untreated and Mitsui-7-treated PCLS. Scale bar represents 100 μm in (a) and (c); 50 μm in (b) and (d); 20 μm in (e). B) Hyperspectral imaging of PCLS exposed to vehicle only or Mitsui-7 for 12 h. Mitsui-7 fibers appear white in the dark-field image and are colored red in hyperspectral images to show mapping to reference library of CNTs. On the far right, a fiber piercing through the PCLS slice can be seen. Scale bar represents 50 μm .

depends on the feedback signaling received from the changing microenvironment over time. The training and validation datasets were limited in the range of doses and post-exposure time points covered for a given substance. The training set consisted of several bleomycin studies and from the results above, it was clear that PFS17 was most predictive of bleomycin-induced fibrosis. Based on these results, it can be concluded that a large number of datasets derived from standardized platforms and protocols, accurately capturing the diverse universe of pro-fibrotic stressors, a full range of post-exposure time points and exposure doses, are required to achieve robust predictive results with PFS17. Such an enriched database will also aid in expanding the PFS17 gene space with genes that accurately describe the gene and pathway heterogeneity and complementarity involved in the process of lung fibrosis.

Albeit a few, PFS17 was able to accurately classify some MWCNT studies as PF, which included studies with repeated or high dose exposure to Mitsui-7 and NM-401, which are long and needle-like MWCNTs. PFS17 also identified studies involving NRCWE-026 as PF, which is a tangled MWCNT, which is considered inert in terms of inducing fibrosis. Although, acute transcriptional responses to NRCWE-026 have been shown to be milder,^[46] the sub-chronic response to NRCWE-026 are much more pronounced compared to the responses induced by Mitsui-7 or NM-401, suggesting that the fibrotic response to NRCWE-026 may take time to establish but involve the expression of genes represented in PFS17. However,

several other studies investigating less toxic MWCNTs were all correctly identified as NF. At present, there are not many publicly available transcriptomics studies describing ENM-induced lung responses, which is a serious limitation to the conclusions derived in this study. A large repository of transcriptomics data describing gene expression profiles in lungs following exposure to a wide variety of ENMs may be required to increase the sensitivity, accuracy, and predictive efficiency of PFS17 for ENMs.

In addition to assessing PFS17 against the available genomics profiles of mouse lungs exposed to a variety of known pro-fibrotic stressors, the study also assessed applicability of PFS17 for assessing stressor-induced fibrosis using an ex vivo lung organ mimic. Ex vivo organoid mimics represent a model in between in vitro and in vivo, which involve culturing of a tissue slice as opposed to select single cell types. The main advantages of this tissue mimic model are that a tissue slice retains the foundational cytoarchitecture and maintains most cell-to-cell interactions, signaling and metabolic processes, required for the development of a pathology. The results showed that PFS17 was effectively triggered in PCLS following exposure to bleomycin on day 7 post-exposure, which aligned with the histological manifestation of bleomycin-induced fibrotic lesions in PCLS. However, PFS17 was weakly triggered following exposure to MWCNTs, although slight increase in trichrome stain reflective of fibrosis was observed in histological sections on day 7 post-exposure to Mitsui-7. Unlike for bleomycin, which is a soluble substance, the critical event in

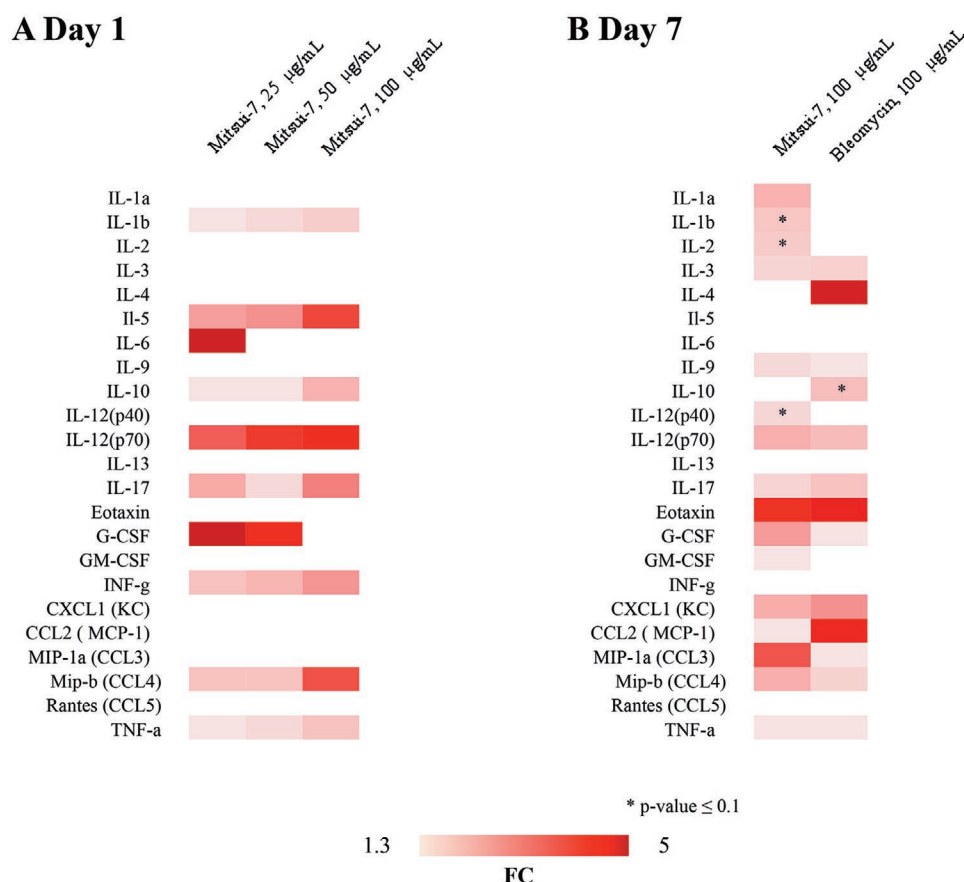


Figure 7. A) Schematic heat map depicting fold changes of 23 cytokine expression via 23-plex cytokine ELISA in supernatant from 250 µm PCLS exposed to 25, 50, and 100 µg mL⁻¹ of Mitsui-7 compared to that of 250 µm PCLS exposed to media control on day 1 post-exposure. B) Schematic heat map depicting fold changes of cytokine expression in lysate from 500 µm PCLS exposed to 100 µg mL⁻¹ of Mitsui-7 and 100 µg mL⁻¹ bleomycin compared to that of PCLS exposed to media control on day 7 post-exposure. Cytokine expressions were quantified using Bioplex assays using three biological replicates. Statistical significance was calculated using Student's *t*-test ($p \leq 0.1$ and fold change ≥ 1.5).

the path of MWCNT-induced lung fibrosis *in vivo* is the interaction between the MWCNT fibers and lung cells. Although, hyperspectral imaging (HSI) showed that MWCNTs interact with PCLS *ex vivo*, the duration of exposure may not have been sufficient to trigger the full-fledged fibrotic responses, or it may require higher doses and/or longer post-exposure time periods for complete manifestation of the response. Additional *ex vivo* experiments were conducted with repeated MWCNT dosing; however, repeated dosing required the change of cell culture medium with each dosing, which resulted in the loss of microenvironment, resetting the biological response (data not shown). Further optimization experiments are warranted to determine the best exposure conditions, dose setting, and post-exposure time points for assessing the applicability of PFS17 in an *ex vivo* model of lung fibrosis.

The PCLS technique has been used and pre-validated for testing inhalation toxicity of chemicals.^[66] However, a majority of these studies used a Krumdieck microtome system that necessitated tissue coring. Although tissue coring enabled harvesting of slices with uniform diameter, often the risk of damaging the health of the slice is high due to the damage incurred during the coring process. Also, this old method of slice generation was manual resulting in heterogeneity in thickness and

surface smoothness of slices. In the present study, PCLS culture technique was optimized as an *ex vivo* alternative to test lung pro-inflammatory and fibrosis pathology induced by ENMs. Specifically, optimal slice thickness for specific endpoints, and short- and long term maintenance, were assessed by the slice viability and the ability to induce physiological markers of lung inflammation and fibrosis, two of the most commonly and consistently observed effects of ENMs in rodent models. The advanced digitalized vibratome used in the present study generated slices of uniform size and thickness without damaging the tissue. Digitalization eliminates the need for expertise and minimizes technical variations introduced by different staff using the equipment, thus enhancing the quality of slices generated, in addition to reproducibility. Since the present study did not core the tissue, lung architecture remained intact in the slices; however, they differed in size and thus, the total surface area. This issue was addressed by normalizing the assay results to the total protein content of the slice.

This study demonstrated that the thin 250 µm slices maintained structural integrity for 48 h; whereas, the thicker 500 µm slices were structurally intact in cultures up to 7 days post-harvesting. This is different to what was shown previously by Neuhaus et al.,^[67] where increasing slice thickness decreased

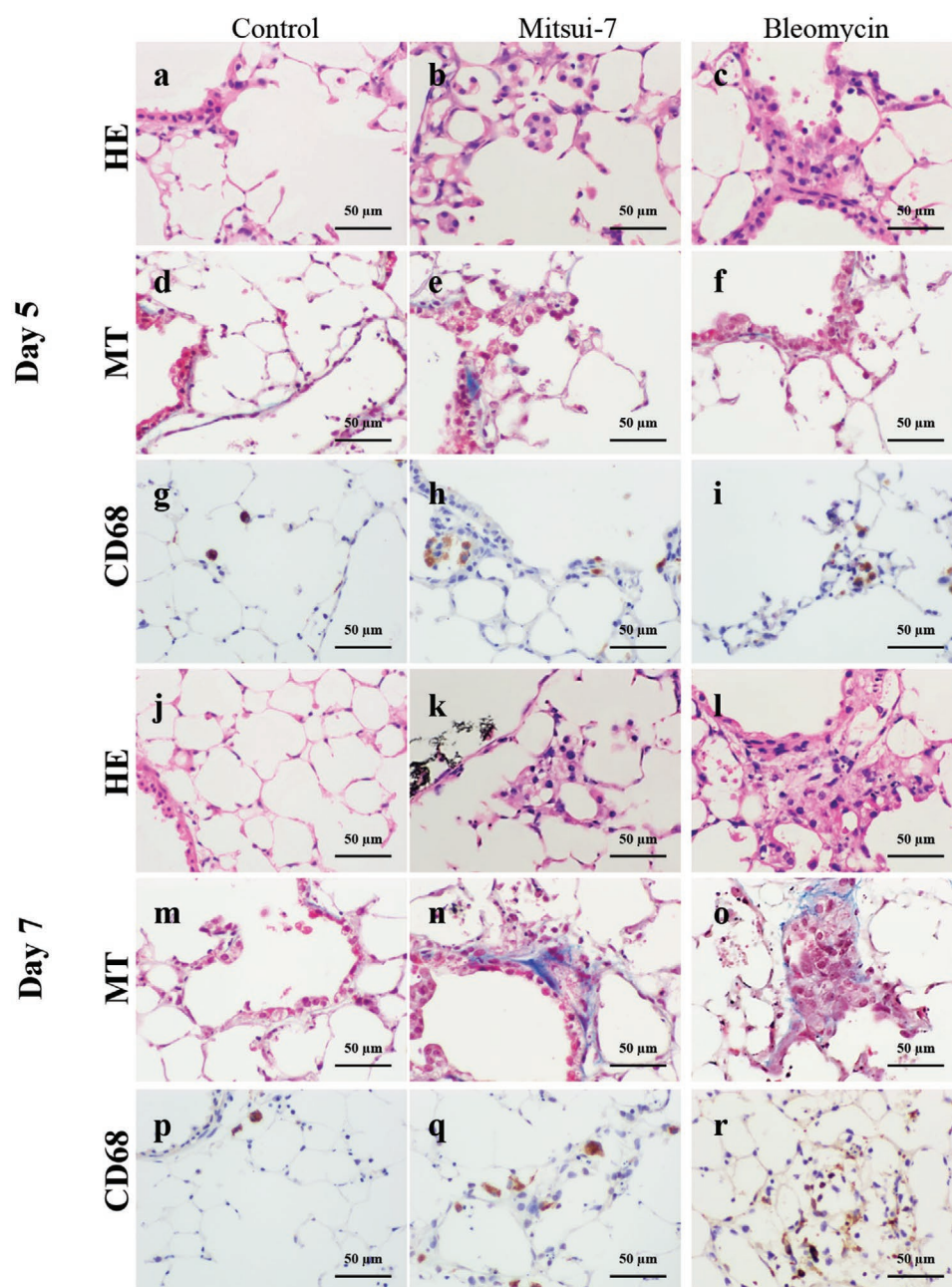


Figure 8. Histopathological analysis of PCLS exposed to vehicle control, Mitsui-7, or bleomycin for morphology (H&E), collagen deposition (Masson trichrome–MT), and resident macrophage activation (CD68), on day 5 and day 7 post-exposure. Scale bar represents 50 μ m.

viability of cells due to reduced oxygen supply owing to reduced diffusion. Although we did not quantitatively assess the levels of oxygen available in the culture medium, morphological analysis of the slice at different post-culture time points did not show any avert loss of cell viability in 500 μ m slices. These results suggested that depending on the endpoint of interest, different slice thicknesses can be used, thus optimizing the maximum number of slices that can be used from one individual animal. One mouse lung (left lobe only) produced up to 18–22 healthy 250 μ m slices, which allowed multiple end-point analyses and cross comparison of dose and/or time effects in the same mouse. The right lobes were also included in the

preliminary optimization phase; however, were found cumbersome to work with in that the small multiple lobes yielded smaller size slices that often necessitated pooling of more than two slices to get enough sample for the assays. Moreover, due to the small size, slicing was also more difficult. Thus, use of right lobes was not deemed useful to perform the assays performed in this study. One of the important objectives of the study was to evaluate the applicability of PCLS to assess ENMs-induced lung inflammation and fibrotic responses. PCLS have been used to assess uptake and cytotoxicity of gold nanoparticles,^[68] induction of inflammatory proteins following exposure to high concentration of silica particles,^[69] and to assess lung responses

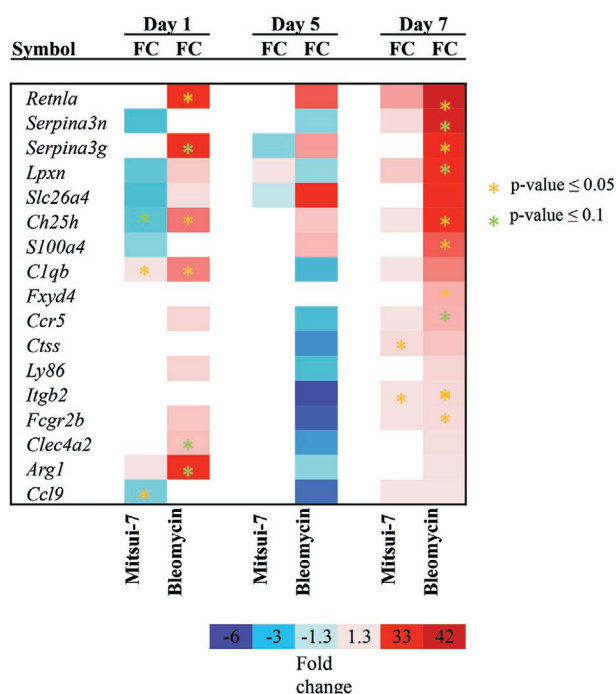


Figure 9. Heatmap showing the qRT-PCR validation results for the differential expression of PFS17 biomarker genes in PCLS following exposure to Mitsui-7 or bleomycin on day 1, day 5, and day 7 post-exposure. The results are normalized to housekeeping genes *Gadph* and *Actb* and expressed as relative fold change compared to matched vehicle exposed controls using three biological replicates.

of exposure to 16 OECD reference ENMs, including titanium dioxide, zinc oxide, cerium oxide, silica, silver, and MWCNTs.^[70] However, none of these studies determined the applicability of PCLS to assess fibrosis. The results of the present study demonstrated that PCLS can be effectively used to screen inflammatory and pro-fibrotic ENMs and non-ENM fibrotic stressors.

In general, the response in PCLS was much higher following exposure to bleomycin compared to the responses induced by MWCNTs. A large number of pro-inflammatory chemokines and cytokines were secreted in the PCLS culture supernatants following a 1 day exposure to a wide variety of ENMs or bleomycin (data not shown). In the lung, the fibrotic process involves activation, recruitment, differentiation and transformation of different cell types, secretion of several pro-inflammatory cytokines, growth and repair factors, and synthesis and accumulation of ECM components, all of which create a microenvironment that engages in intricate signaling during the process leading eventually to wound healing and the repair process. Because of this complexity, animal testing is the preferred choice for assessing fibrosis. Although the present ex vivo model did not allow the assessment of infiltrating monocytes, using histological analysis, the study showed recruitment of resident immune cells to the site of injury, activation of macrophages (Figure 8b–c,k–l), presence of fibroblasts (Figure 8h–i,q–r), and increased deposition of collagen (Figure 8e–f,n–o), the hall mark events of the fibrotic process. Although, in general the response to ENMs was weaker in all the endpoints assessed compared to the response induced by bleomycin, the results conclusively showed the sensitivity of

the technique as an alternative to whole animal testing for the assessment of pro-fibrotic stressors.

The PFS17 is derived from animal experimentation and thus not fully transferable to human models. However, one of the attractive features of the ex vivo model is the future possibility of using human tissue slices from tissue banks. The PFS17 genes have human homologues and most are shown to be involved in human pro-fibrotic responses. For example, in a study by Roach et al., families of serine (or cysteine) proteinase inhibitor genes—*SERPINE1*, *SERPINH1*, *SERPINA1*; integrins—*ITGB5*, *ITGB8*; and a chemokine receptor—*CCR2*, were shown to be differentially expressed in *TGFB* stimulated precision-cut lung tissue slices that were derived from patients with idiopathic fibrosis.^[71] In another study by Wright et al., leupaxin C type lectin, natural killer cell receptor family (*CLEC2D*), calcium binding protein coding gene *S100A16*, and Na/H exchanger (*FXYD2*) were differentially expressed in nasal respiratory epithelial cells collected from patients with cystic fibrosis.^[72] Gene expression analysis of lung tissue from patients with systemic sclerosis presenting with severe pulmonary fibrosis showed differential expression of *TGFB1*, calcium binding protein 4A (*S100A4*), and solute carrier organic anion transporter family (*SLCO2A1*).^[73] Genes encoding calcium binding protein; serine (or cysteine) proteinase inhibitor; clade E (*SERPINE2*) and solute carrier family 34, member 2 (*SLC34A2*); solute carrier family 6, member 4 (*SLC6A4*); solute carrier family 6, member 14 (*SLC6A14*); and resistin (*RETN*) were found differentially expressed in lung tissue samples from patients with idiopathic pulmonary fibrosis.^[74] Noguchi et al. showed that genes encoding calcium binding protein (*S100A10*) and solute carrier family 7 members (*SLC7A14*, *SLC7A5*) were differentially expressed in human lung fibroblast cells transfected with TAZ (Transcriptional coactivator with PDZ-binding motif) siRNA.^[75] The expression of cholesterol 25 hydroxylase (*CH25H*) is upregulated in human lung primary fibroblasts following stimulation with eosinophils.^[76] Several studies have shown detectable level of cathepsin S (*Ctss*) in the airways of patients with cystic fibrosis.^[77] Thus, many of the genes from PFS17 are associated with lung fibrosis disease in humans. Further work is underway to expand PFS17 and to validate its applicability to predict fibrotic responses in humans. In concluding, the ex vivo model is effective in delivering the 3Rs principles; however, it is not a perfect alternative to a whole animal study and has its own limitations. Although it preserves the lung architecture with all the cell types in their original morphological and functional state, the dynamic defense and repair mechanisms of an organ may not be fully replicated ex vivo. While ex vivo system makes cross species investigation easier, the limitation is that each individual organ has to be separately studied. Thus, in the current search for effective animal alternatives, the value of traditional animal studies that offer systematic investigation of systemic responses of all possible organ systems impacted by the exposure cannot be understated.

4. Conclusions

In this proof-of-principle study, we have established a transcriptomics biomarker panel PFS17 to predict stressor-induced

fibrosis that can be applied to screening the pro-fibrotic ENMs and non-nano substances. The study also optimized an ex vivo lung organ mimic system for assessing ENMs-induced fibrosis. Conditional to further optimization, the combination of the PFS17 biomarker and the ex vivo lung mimic system is a robust and promising alternative for screening thousands of stressors, including ENMs, for their fibrogenic potential. The PFS17 biomarker is anchored to the key events identified in the AOP173 and thus offers mechanistic information on genomics responses associated with the fibrotic process. With further optimization, this experimental combination offers a medium throughput testing strategy that is a resource and cost effective alternative to whole animal testing.

5. Experimental Section

Collection of Microarray Datasets and Data Processing: All data used in the study are publicly available and were obtained from the Gene Expression Omnibus (GEO). The accession numbers for the studies^[19–24] used in the development of the gene signature are presented in Table 1. The datasets represent a variety of lung diseases and lung injury outcomes, including lung inflammation, emphysema, COPD, and lung cancer. The individual microarray platforms used in the studies differed and included the Illumina expression beadchip, oligo arrays, and Affymetrix. For the two color microarray studies, the LOWESS normalization method^[78] using the R statistical software environment was applied.^[79] The RMA normalization was applied using the justRMA function in the affy^[80] R package for studies using the Affymetrix GeneChips. Quantile normalization was applied for studies that utilized the Illumina beadchip using the lumiN function in the lumi R package.^[81] The normalized signal intensities were log2 transformed and probes with technical replicates were averaged using the median, and the data were further collapsed using the gene symbol. Each sample condition was then averaged to the group median and then normalized to the appropriate control samples.

Bi-Clustering Analysis: The detailed methodology was published previously.^[16,17] Briefly, the bi-clustering data analysis was conducted in R using the biclust package.^[82] The repeated Bimax method was selected for this analysis.^[83] Bimax uses a simple data model that assumes two possible states for each expression level, no change and change with respect to a control experiment. For this analysis, two binary matrices were constructed: one matrix, consisting of zeros and ones, where the ones indicated genes that were twofold up-regulated and a second matrix, where the ones identify genes that were twofold down-regulated.

The option for the minimum number of rows for the Bimax method was set at 15. The minimum number of columns (which represent the experimental conditions) was set as 5 and the maximum number of columns was set as 15. This resulted in eight bi-clusters from the binary matrix representing the up-regulated genes and two bi-clusters were identified for the matrix representing the down-regulated genes.^[16]

Development of a Pro-Fibrotic Signature: Of the eight bi-clusters (from above), one of them consisting of 17 genes and experimental samples related to the T helper type 2 (Th2) response, bacterial infection, asthma, and pulmonary fibrosis was further evaluated for shrunken centroid analysis (SCA).^[84] Activation of Th2 response pathways, bacterial infection and asthmatic conditions are known to favour the development of lung fibrosis. The class (pro-fibrotic – PF or non-fibrotic – NF) labels were defined by the samples that constituted the bi-cluster and additional samples were added to the PF class which had a subset of expressed genes that were common to bi-cluster but did not meet the inclusion criteria used in defining the bi-clustering algorithm. SCA was then conducted in R using the pamr library using these genes,^[85] and sample labels were then used to estimate the centroids for the predictive model.

Validation of the Pro-Fibrotic Signature: Independently conducted, publicly available data were obtained from GEO to validate the 17-gene PF biomarker panel (PFS17). Studies involving exposures to potential PF stressors, such as bleomycin, ozone, radiation, and MWCNTs, were downloaded from the public domain, processed, and normalized as described above. For the Illumina HiSeq 2500 platform, counts per million was used to estimate gene expression and biological replicates for each experimental condition were averaged using the median.

The PFS17 was then applied to each of these studies. The probability of class membership was estimated using the analogy to the Gaussian linear discriminate.^[84] Samples with PF class probabilities greater than 0.8 were classified as PF and samples with PF class probabilities less than 0.2 were classified as NF. Samples with class probabilities between 0.2 and 0.8 were classified as unknown. Heatmaps with the training set and each of the individual studies were utilized to visualize the predictions.

Animal Care, Handling, Sacrifice, and PCLS Generation: C57BL/6 female mice aged 6–8 weeks were obtained from Charles River (St Constant, QC, Canada) and were housed under pathogen-free conditions using a 12 h:12 h light/dark cycle with food and water available ad libitum. The mice were allowed to acclimatize for at least 3–5 days before necropsy. All animal procedures were conducted in accordance with the guidelines of the Canadian Council for Animal Care and approved by the Health Canada Animal Care Committee.

Control unexposed mice were anesthetized under isoflurane and euthanized by cervical dislocation. Post mortem, the trachea was gradually filled with 1.5 mL of a 1:1 ratio of 4% low gelling temperature agarose (Sigma Aldrich, Oakville, ON, Canada) and 1X Hank's Balanced Salt Solution (HBSS) (Gibco, Burlington, ON, Canada) at 40 °C, followed by a 0.2 mL injection of air to inflate the lungs. Gauze saturated with chilled 1X HBSS was placed over the lungs and the mouse was incubated on ice for a minimum of 15 min. Once cooled, the lungs were extracted and placed in a petri dish covered with chilled 1X HBSS saturated gauze and then placed on ice until slicing was conducted.

PCLS were generated using the VT1200 S vibrating-blade microtome (Leica Biosystems, 14048180101 RevC; Concord, ON, Canada) as per the manual. Using super glue, the lung lobe was mounted on the specimen plate denoted for specimens 2 cm in height, with the lung branches facing upward and the buffer tray was filled with chilled 1X HBSS. The blade feed rate was set at 0.60 min s^{−1}, the amplitude at 1.00 mm, and the section thickness at 250 or 500 µm. Each slice was then placed in chilled 1X HBSS. The left lung lobe was preferred as it is a single large lobe compared to the multi-lobe right lung; it is easier to manipulate and provides larger slices. Figure S39, Supporting Information, represents a schematic diagram for lung slice generation.

PCLS Culture: Following sectioning, the PCLS were incubated at 37 °C for 45 min, after which slices were washed every hour for a total of three times using lung slice media (Dulbecco's Modified Eagle Medium/ Nutrient Mixture F-12; Gibco, Burlington, ON, Canada) supplemented with 35 µg mL^{−1} L-ascorbic acid (Sigma-Aldrich, Oakville, ON, Canada), 5 µg mL^{−1} transferrin (bovine, Halo form; Gibco, Burlington, ON, Canada), 2.85 µg mL^{−1} insulin from bovine pancreas (Sigma-Aldrich, Oakville, ON, Canada), 3.2 pg mL^{−1} selenium (Fluka, Oakville, ON, Canada), 250 ng mL^{−1} of amphotericin B (Sigma-Aldrich, Oakville, ON, Canada), and 5 mL of Pen-Strep (Gibco, Burlington, ON, Canada).

Preparation of Mitsui-7 and Bleomycin for Exposure: The stock suspensions of Mitsui-7, bleomycin, LPS, and lysis buffer were prepared fresh each time immediately before the exposure. The stock suspensions of MWCNTs were prepared in MilliQ water containing 2% serum prepared from C57BL/6 mice at a concentration of 1 mg mL^{−1}. Suspensions were sonicated at 40 W on ice using the S-450D sonifier (Branson Ultrasonics Corporation, Danbury, CT, USA) equipped with a disrupter horn (model number: 101-147-037) in an enclosed chamber. To ensure dispersions, MWCNTs in MilliQ water containing 2% serum were sonicated for 16 min without any pulse. The stock was diluted further in the lung slice medium to obtain different exposure concentrations of 25, 50, and 100 µg mL^{−1}. The dilutions were sonicated for an additional minute on ice before exposing PCLS. Dilutions of bleomycin (100 µg mL^{−1}) were prepared in

lung slice medium from 2 mg mL⁻¹ bleomycin stock in phosphate buffer saline; stock solutions of LPS (1 µg mL⁻¹) and lysis (10% Triton X-100) buffer were prepared in lung slice medium.

PCLS Exposure: Following the washes, the PCLS were acclimatized overnight in a 24-well cell culture plate, with a single slice per well in 0.5 mL lung slice media. Occasionally, two smaller-sized slices were cultured together in a single well. The lung slice media was carefully removed from wells with a pipette following 24 h incubation and replaced with 0.5 mL of fresh suspensions of ENM, chemicals, or exposure vehicle only (control untreated slices). Different experimental controls were used; 1 µg mL⁻¹ of LPS, a known pro-inflammatory endotoxin, was used as a positive control in experiments targeting inflammatory reactions. For cytotoxicity experiments, 10% Triton X-100 (Thermo-Fisher Scientific, BP151500, Burlington, ON, Canada) served as a positive control. Following treatment with stressors, the lung slices were returned to the incubator at 37 °C. Lung slices and the supernatant were harvested at different post-exposure time points and stored at -80 °C until processed for the specific assays.

Hyperspectral Imaging of PCLS Exposed to Mitsui-7: Tissue slices for histology were prepared and a hyperspectral imaging (HSI) system was used to visualize Mitsui-7 fibers in PCLS in accordance with the protocols described previously.^[9] Briefly, HSI of H&E stained PCLS samples stimulated with Mitsui-7 were taken at 100× magnification using a CytoViva nanoscale hyperspectral microscope with a detection range of 400–1000 nm (CytoViva, Inc., Auburn, AL, USA). The images were analyzed using the Environment for Visualization (ENVI 4.8; CytoViva, Inc. Auburn, AL, USA) software. The spectra from the Mitsui-7 stimulated samples were compared to a reference spectral library created for Mitsui-7 by spectral angle mapping, a spectral classification algorithm in ENVI that uses an n-D angle to match pixels from the stimulated samples to reference spectra. An n-D angle equal or lower than the maximum threshold of 0.15 radian represents 100% match to the reference sample.^[14]

Total Protein Extraction and Quantification: Frozen tissue slices were homogenized in cell lysis solution with a 5 mm Retsch stainless steel bead (Thermo-Fisher Scientific, Burlington, ON, Canada).

Cell lysis solution was assembled using multiple components (factor 1 and 2; BioRad, Mississauga, ON) and protease inhibitor (Sigma-Aldrich, Oakville, ON, Canada).

Samples were homogenized twice using pre-chilled Retsch Mixer Mill MM 400 adapters at 25 Hz for 1 min. The procedure was repeated the second time with incubation on ice for 1 min between homogenizations. The homogenates were incubated on ice for 20 min with regular agitation at 5 min intervals. Samples were centrifuged twice at 8000 rpm at 4 °C for 10 min to ensure complete removal of MWCNTs. The supernatant above the MWCNT pellet was removed and stored at -80 °C until use.

Total protein from each sample was quantified using the bicinchoninic acid (BCA) assay, using bovine serum albumin (BSA) as the standard, as per the manufacturer's instruction for the microplate procedure (Pierce, Rockland, IL). The sample was diluted 1:10 in 1X Dulbecco's phosphate-buffered saline solution (Gibco, Burlington, ON, Canada) and serial dilutions of the standard were prepared in the same solution. Absorbance was read at 562 nm using a microplate reader.

Cytotoxicity Assessment: Cells with compromised membrane integrity release LDH, which is used as an indicator of cell death. Thus, the percentage of cell death is proportional to the percentage of LDH released by the cells in the supernatant. In brief, 10 µL of supernatant from each sample and standards were loaded into individual wells of 96-well plate, followed by the substrate mix (LDH assay kit by Abcam, Toronto, ON, Canada). Absorbance was measured at 490 nm, with a reference wavelength of 600 nm. LDH release was normalized to the protein content of the corresponding PCLS lysate and expressed in terms of fold change compared to media control. Lysis buffer was used as a positive control for cytotoxicity. All assays were conducted in three biological replicates.

Measurement of Cytokines via Bio-Plex Pro Assays: The levels of pro-inflammatory and pro-fibrotic cytokines were determined using a 23 Plex

panel of Bio-Plex Pro Mouse Cytokine assay (BioRad, Mississauga, Canada). The specific cytokines included: IL-1α, IL-1β, IL-2, IL-3, IL-4, IL-5, IL-6, IL-9, IL-10, IL-12 p40, IL-12 p70, IL-13, IL-17, eotaxin, G-CSF, GM-CSF, INF-γ, KC, MCP-1, MIP-1α, MIP-1β, RANTES, and TNF-α. The assay was performed according to the manufacturer's instructions. Both the standard diluent (lung slice media) and PCLS supernatants (after the removal of MWCNTs by centrifugation) were prepared in 0.5% w/v bovine serum albumin, BSA (Sigma-Aldrich, A-9647, Oakville, ON, Canada) to stabilize protein analytes and to prevent adsorption onto labware. The plates were washed using a manual vacuum manifold. Concentration of each chemokine/cytokines was obtained using the Bioplex Manager Software (version 6), which uses calibration curves obtained from a fourfold serial dilution of standards. For the analysis of proteins in the supernatants, concentrations of each chemokine/cytokines in the supernatant were normalized to total protein in the corresponding PCLS. In contrast, for the analysis of proteins from lysate, a total of 25 µg of protein extracted from each PCLS sample ($n = 3$, from three individual mice) was used in the assay and each sample was run twice (two technical replicates).

Quantification of Pro-Fibrotic Markers OPN, TGF-β, and CCL-2: The expression of pro-fibrotic markers OPN, TGF-β, and chemokine (C-C motif) ligand 2 (CCL-2) were measured in the supernatants using commercially available mouse enzyme-linked immunosorbent assay kits (Quantikine ELISA, R&D Systems, Minneapolis, MN, USA). ELISAs were performed according to the manufacturer's specifications. The lower limit of detection for OPN, TGF-β, and CCL-2 was 39, 31.3, and 15.6 pg mL⁻¹, respectively. Absorbance was determined at 450 nm with a reference wavelength at 540 nm.

Histopathology: The PCLS from control and treated groups ($n = 3$) were fixed in 10% formalin for 24 h, paraffin embedded, cut into 4 mm thick sections and stained with H&E or Masson trichrome to assess inflammation and collagen deposition, respectively. The paraffin-embedded PCLS were also stained with macrophage marker CD68 (Rabbit CD68; Abcam, Toronto, ON, Canada). Immunostaining with CD68 was conducted according to the manufacturer's protocol. The service was carried out in the PALM Histology Core Facility, University of Ottawa, Ottawa, Ontario, Canada.

Assessment of PFS17 in PCLS: A custom quantitative real-time (qRT)-PCR array (CLAM28143_ QIAGEN Sciences, Maryland, USA) was designed to assess the expression of PFS17 in PCLS following exposure to pro-fibrotic substances. PCLS were harvested and treated with MWCNT Mitsui-7 and bleomycin, the two well-studied pro-fibrotic substances included in this study. A total of 0.8 µg of total RNA from each PCLS sample exposed to vehicle only, Mitsui-7, or bleomycin was reverse transcribed using the RT² first strand kit (QIAGEN Sciences, Maryland, USA). The qRT-PCR was conducted using a BioRad CFX96 Real-Time PCR detection system using a RT² SYBR Green qPCR Mastermix (QIAGEN Sciences, Maryland, USA). Data were normalized to hypoxanthine-guanine phosphoribosyltransferase (*Hprt*), actin β (*Actb*), and glyceraldehyde 3-phosphate dehydrogenase (*Gapdh*) reference genes, which were chosen based on their stable expression levels in mouse lungs in previous studies.^[86] Relative expression of genes was calculated using the online PCR array data analysis software (QIAGEN Sciences, Maryland, USA).

Supporting Information

Supporting Information is available from the Wiley Online Library or from the author.

Acknowledgements

L.R. and A.W. contributed equally to this work. This work was supported by the Health Canada's Genomics Research and Development Initiative and Chemicals Management Plan2-nano.

Conflict of Interest

The authors declare no conflict of interest.

Keywords

advanced lung exposure models, bi-clustering, fibrosis, lung pathology, organoid culture, predictive gene signature

Received: January 14, 2020

Revised: March 23, 2020

Published online: April 29, 2020

- [1] C. L. Geraci, V. Castranova, *Wiley Interdiscip. Rev.: Nanomed. Nanobiotechnol.* **2010**, 2, 569.
- [2] H. Johnston, G. Pojana, S. Zuin, N. R. Jacobsen, P. Møller, S. Loft, M. Semmler-Behnke, C. McGuiness, D. Balharry, A. Marcomini, *Crit. Rev. Toxicol.* **2013**, 43, 1.
- [3] A. D. Maynard, D. B. Warheit, M. A. Philbert, *Toxicol. Sci.* **2011**, 120, S109.
- [4] A. Noel, K. Maghni, Y. Cloutier, C. Dion, K. J. Wilkinson, S. Halle, R. Tardif, G. Truchon, *Toxicol. Lett.* **2012**, 214, 109.
- [5] D. B. Warheit, T. R. Webb, K. L. Reed, S. Frerichs, C. M. Sayes, *Toxicology* **2007**, 230, 90.
- [6] S. J. Evans, M. J. D. Clift, N. Singh, J. de Oliveira Mallia, M. Burgum, J. W. Wills, T. S. Wilkinson, G. J. S. Jenkins, S. H. Doak, *Mutagenesis* **2017**, 32, 233.
- [7] S. Halappanavar, A. T. Saber, N. Decan, K. A. Jensen, D. Wu, N. R. Jacobsen, C. Guo, J. Rogowski, I. K. Koponen, M. Levin, *Environ. Mol. Mutagen.* **2015**, 56, 245.
- [8] M. Husain, A. T. Saber, C. Guo, N. R. Jacobsen, K. A. Jensen, C. L. Yauk, A. Williams, U. Vogel, H. Wallin, S. Halappanavar, *Toxicol. Appl. Pharmacol.* **2013**, 269, 250.
- [9] J. Nikota, A. Banville, L. R. Goodwin, D. Wu, A. Williams, C. L. Yauk, H. Wallin, U. Vogel, S. Halappanavar, *Part. Fibre Toxicol.* **2017**, 14, 37.
- [10] S. S. Poulsen, P. Jackson, K. Kling, K. B. Knudsen, V. Skaug, Z. O. Kyjovska, B. L. Thomsen, P. A. Clausen, R. Atluri, T. Berthing, *Nanotoxicology* **2016**, 10, 1263.
- [11] S. S. Poulsen, K. B. Knudsen, P. Jackson, I. E. Weydahl, A. T. Saber, H. Wallin, U. Vogel, *PLoS One* **2017**, 12, e0174167.
- [12] S. S. Poulsen, N. R. Jacobsen, S. Labib, D. Wu, M. Husain, A. Williams, J. P. Bøgelund, O. Andersen, C. Købler, K. Mølhave, *PLoS One* **2013**, 8, e80452.
- [13] L. Rahman, D. Wu, M. Johnston, A. Williams, S. Halappanavar, *Mutagenesis* **2017**, 32, 59.
- [14] L. Rahman, N. R. Jacobsen, S. A. Aziz, D. Wu, A. Williams, C. L. Yauk, P. White, H. Wallin, U. Vogel, S. Halappanavar, *Mutat. Res.,/Genet. Toxicol. Environ. Mutagen.* **2017**, 823, 28.
- [15] J. Nikota, A. Williams, C. L. Yauk, H. Wallin, U. Vogel, S. Halappanavar, *Part. Fibre Toxicol.* **2015**, 13, 25.
- [16] A. Williams, S. Halappanavar, *Beilstein J. Nanotechnol.* **2015**, 6, 2438.
- [17] A. Williams, S. Halappanavar, *Data Brief* **2017**, 15, 933.
- [18] S. Labib, A. Williams, C. L. Yauk, J. K. Nikota, H. Wallin, U. Vogel, S. Halappanavar, *Part. Fibre Toxicol.* **2015**, 13, 15.
- [19] C. C. Lewis, J. Y. H. Yang, X. Huang, S. K. Banerjee, M. R. Blackburn, P. Baluk, D. M. McDonald, T. S. Blackwell, V. Nagabhushanam, W. Peters, D. Voehringer, D. J. Erle, *Am. J. Respir. Crit. Care Med.* **2008**, 177, 376.
- [20] R. S. Thomas, L. Pluta, L. Yang, T. A. Halsey, *Toxicol. Sci.* **2007**, 97, 55.
- [21] X. Lu, V. V. Jain, P. W. Finn, D. L. Perkins, *Mol. Syst. Biol.* **2007**, 3, 98.
- [22] T. Rangasamy, V. Misra, L. Zhen, C. G. Tankersley, R. M. Tudor, S. Biswal, *Am. J. Physiol. Lung Cell. Mol. Physiol.* **2009**, 296, L888.
- [23] E. M. Thomson, A. Williams, C. L. Yauk, R. Vincent, *Am. J. Pathol.* **2012**, 180, 1413.
- [24] B. E. Schaffer, K. S. Park, G. Yiu, J. F. Conklin, C. Lin, D. L. Burkhardt, A. N. Karnezis, E. A. Sweet-Cordero, J. Sage, *Cancer Res.* **2010**, 70, 3877.
- [25] C. E. Ochoa, S. G. Mirabolfathinejad, V. A. Ruiz, S. E. Evans, M. Gagea, C. M. Evans, B. F. Dickey, S. J. Moghaddam, *Cancer Prev. Res.* **2011**, 4, 51.
- [26] T. Liu, H. A. Baek, H. Yu, H. J. Lee, B. H. Park, M. Ullenbruch, J. Liu, T. Nakashima, Y. Y. Choi, G. D. Wu, M. J. Chung, S. H. Phan, *J. Immunol.* **2011**, 187, 450.
- [27] A. R. Pandiri, R. C. Sills, V. Ziglioli, T. V. Ton, H.-H. L. Hong, S. A. Lahousse, K. E. Gerrish, S. S. Auerbach, K. R. Shockley, P. R. Bushel, *Toxicol. Pathol.* **2012**, 40, 1141.
- [28] R. Peng, S. Sridhar, G. Tyagi, J. E. Phillips, R. Garrido, P. Harris, L. Burns, R. Renteria, J. Woods, L. Chen, J. Allard, P. Ravindran, H. Bitter, Z. Liang, C. M. Hogaboam, C. Kitson, D. C. Budd, J. S. Fine, C. M. Bauer, C. S. Stevenson, *PLoS One* **2013**, 8, e59348.
- [29] O. Delgado, K. G. Batten, J. A. Richardson, X. J. Xie, A. F. Gazdar, A. A. Kaisani, L. Girard, C. Behrens, M. Suraokar, G. Fasciani, *Clin. Cancer Res.* **2014**, 20, 1610.
- [30] G. John-Schuster, K. Hager, T. M. Conlon, M. Irmeler, J. Beckers, O. Eickelberg, A. Ö. Yildirim, *Am. J. Physiol. Lung Cell. Mol. Physiol.* **2014**, 307, L692.
- [31] S. Knippenberg, B. Ueberberg, R. Maus, J. Bohling, N. Ding, M. T. Tarres, H. G. Hoymann, D. Jonigk, N. Izykowski, J. C. Paton, *Thorax* **2015**, 70, 636.
- [32] T. R. Cox, J. T. Erler, *Clin. Cancer Res.* **2014**, 20, 3637.
- [33] C. L. Lino Cardenas, I. S. Henaoui, E. Courcot, C. Roderburg, C. Cauffiez, A. Sébastien, M. C. Copin, B. Wallaert, F. Glowacki, E. Dewaeles, J. Milosevic, J. Maurizio, J. Tedrow, B. Marcet, J. M. Lo-Guidice, N. Kaminski, P. Barbry, T. Luedde, M. Perrais, B. Mari, N. Pottier, *PLoS Genet.* **2013**, 9, e1003291.
- [34] A. K. Bauer, E. A. Rondini, K. A. Hummel, L. M. Degraff, C. Walker, A. E. Jedlicka, S. R. Kleeberger, *Environ. Health Perspect.* **2011**, 119, 1091.
- [35] G. S. Backus, R. Howden, J. Fostel, A. K. Bauer, H. Y. Cho, J. Marzec, D. B. Peden, S. R. Kleeberger, *Environ. Health Perspect.* **2010**, 118, 1721.
- [36] J. M. Ciencewicki, K. C. Verhein, K. Gerrish, Z. R. McCaw, J. Li, P. R. Bushel, S. R. Kleeberger, *Am. J. Physiol. Lung Cell. Mol. Physiol.* **2016**, 311, L280.
- [37] T. Moritake, H. Fujita, M. Yanagisawa, M. Nakawatari, K. Imadome, E. Nakamura, M. Iwakawa, T. Imai, *Int. J. Radiat. Oncol., Biol., Phys.* **2012**, 84, e95.
- [38] D. E. Citrin, U. Shankavaram, J. A. Horton, W. Shield III, S. Zhao, H. Asano, A. White, A. Sowers, A. Thetford, E. J. Chung, *JNCI, J. Natl. Cancer Inst.* **2013**, 105, 1474.
- [39] I. L. Jackson, F. Baye, C. P. Goswami, B. P. Katz, A. Zodda, R. Pavlovic, G. Gurung, D. Winans, Z. Vujaskovic, *Dis. Models Mech.* **2017**, 10, 425.
- [40] T. A. Beach, A. M. Groves, C. J. Johnston, J. P. Williams, J. N. Finkelstein, *Int. J. Radiat. Biol.* **2018**, 94, 1104.
- [41] N. L. Guo, Y. W. Wan, J. Denvir, D. W. Porter, M. Pacurari, M. G. Wolfarth, V. Castranova, Y. Qian, *J. Toxicol. Environ. Health A* **2012**, 75, 1129.
- [42] E. M. Rydman, M. Ilves, A. J. Koivisto, P. A. S. Kinaret, V. Fortino, T. S. Savinko, M. T. Lehto, V. Pulkkinen, M. Vippola, K. J. Hämmeri, S. Matikainen, H. Wolff, K. M. Savolainen, D. Greco, H. Alenius, *Part. Fibre Toxicol.* **2014**, 11, 48.
- [43] S. S. Poulsen, A. T. Saber, A. Williams, O. Andersen, C. Købler, R. Atluri, M. E. Pozzebon, S. P. Mucelli, M. Simion, D. Rickerby, *Toxicol. Appl. Pharmacol.* **2015**, 284, 16.
- [44] S. Halappanavar, L. Rahman, J. Nikota, S. S. Poulsen, Y. Ding, P. Jackson, H. Wallin, O. Schmid, U. Vogel, A. Williams, *NanoImpact* **2019**, 14, 100158.

- [45] D. W. Porter, A. F. Hubbs, R. R. Mercer, N. Wu, M. G. Wolfarth, K. Sriram, S. Leonard, L. Battelli, D. Schwegler-Berry, S. Friend, *Toxicology* **2010**, 269, 136.
- [46] S. S. Poulsen, A. T. Saber, A. Williams, O. Andersen, C. Kobler, R. Atluri, M. E. Pozzebon, S. P. Mucelli, M. Simion, D. Rickerby, A. Mortensen, P. Jackson, Z. O. Kyjovska, K. Molhave, N. R. Jacobsen, K. A. Jensen, C. L. Yauk, H. Wallin, S. Halappanavar, U. Vogel, *Toxicol. Appl. Pharmacol.* **2015**, 284, 16.
- [47] J. Dong, Q. Ma, *Arch. Toxicol.* **2016**, 90, 2231.
- [48] J. Knust, M. Ochs, H. Gundersen, J. Nyengaard, *Anat. Rec.* **2009**, 292, 113.
- [49] C. E. L. Chua, Y. S. Lim, M. G. Lee, B. L. Tang, *J. Cell. Physiol.* **2012**, 227, 3722.
- [50] H. Zhang, P. Wu, F. Chen, Y. Hao, Y. Lao, L. Ren, L. Sun, W. Sun, H. Wei, D. W. Chan, *Proteomics* **2014**, 14, 1977.
- [51] S. Kolahian, I. E. Fernandez, O. Eickelberg, D. Hartl, *Am. J. Respir. Cell Mol. Biol.* **2016**, 55, 309.
- [52] Y. Chen, Y. Yang, B. Xu, S. Wang, B. Li, J. Ma, J. Gao, Y. Y. Zuo, S. Liu, *J. Environ. Sci.* **2017**, 62, 100.
- [53] R. J. Snyder, S. Hussain, C. J. Tucker, S. H. Randell, S. Garantziotis, *Part. Fibre Toxicol.* **2017**, 14, 44.
- [54] K. S. Duke, J. C. Bonner, *Wiley Interdiscip. Rev.: Nanomed. Nanobio-technol.* **2018**, 10, e1498.
- [55] Z. Chen, Q. Wang, M. Asmani, Y. Li, C. Liu, C. Li, J. M. Lippmann, Y. Wu, R. Zhao, *Sci. Rep.* **2016**, 6, 31304.
- [56] D. C. Davidson, R. Derk, X. He, T. A. Stueckle, J. Cohen, S. V. Pirela, P. Demokritou, Y. Rojanasakul, L. Wang, *Part. Fibre Toxicol.* **2015**, 13, 23.
- [57] T. A. Wynn, *J. Clin. Invest.* **2007**, 117, 524.
- [58] F. Nimmerjahn, J. V. Ravetch, in *Advances in Immunology*, 96 edn., Academic Press, San Diego, CA **2007**, p. 179.
- [59] E. Addis-Lieser, J. Köhl, M. G. Chiaramonte, *J. Immunol.* **2005**, 175, 1894.
- [60] N. Dharajiya, S. V. Vaidya, H. Murai, V. Cardenas, A. Kurosky, I. Boldogh, S. A. Sur, *PLoS One* **2010**, 5, e9337.
- [61] A. Capelli, A. Di Stefano, I. Gnemmi, C. F. Donner, *Eur. Respir. J.* **2005**, 25, 701.
- [62] L. Barron, A. M. Smith, K. C. El Kasmi, J. E. Qualls, X. Huang, A. Cheever, L. A. Borthwick, M. S. Wilson, P. J. Murray, T. A. Wynn, *PLoS One* **2013**, 8, e61961.
- [63] J. T. Pesce, T. R. Ramalingam, M. S. Wilson, M. M. Mentink-Kane, R. W. Thompson, A. W. Cheever, J. F. Urban Jr., T. A. Wynn, *PLoS Pathog.* **2009**, 5, e1000393.
- [64] T. Raselli, A. Wyss, M. N. Gonzalez Alvarado, B. Weder, C. Mamie, M. R. Spalinger, W. T. Van Haaften, G. Dijkstra, A. W. Sailer, P. H. Imenez Silva, C. A. Wagner, V. Tosevski, S. Leibl, M. Scharl, G. Rogler, M. Hausmann, B. Misselwitz, *J. Crohn's Colitis* **2019**, 13, 1186.
- [65] J. C. Mar, N. A. Matigian, J. Quackenbush, C. A. Wells, *PLoS One* **2011**, 6, e25445.
- [66] A. Hess, L. Wang-Lauenstein, A. Braun, S. N. Kolle, R. Landsiedel, M. Liebsch, L. Ma-Hock, R. Pirow, X. Schneider, M. Steinfath, *Toxicol. In Vitro* **2016**, 32, 347.
- [67] V. Neuhaus, D. Schaudien, T. Golovina, U. A. Temann, C. Thompson, T. Lippmann, C. Bersch, O. Pfennig, D. Jonigk, P. Braubach, *J. Occup. Med. Toxicol.* **2017**, 12, 13.
- [68] S. Dragoni, G. Franco, M. Regoli, M. Bracciali, V. Morandi, G. Sgaragli, E. Bertelli, M. Valoti, *Toxicol. Sci.* **2012**, 128, 186.
- [69] V. Neuhaus, K. Schwarz, A. Klee, S. Seehase, C. Förster, O. Pfennig, D. Jonigk, H. G. Fieguth, W. Koch, G. Warnecke, *PLoS One* **2013**, 8, e71728.
- [70] U. G. Sauer, S. Vogel, A. Aumann, A. Hess, S. N. Kolle, L. Ma-Hock, W. Wohlleben, M. Dammann, V. Strauss, S. Treumann, *Toxicol. Appl. Pharmacol.* **2014**, 276, 1.
- [71] K. M. Roach, A. Sutcliffe, L. Matthews, G. Elliott, C. Newby, Y. Amrani, P. Bradding, *Sci. Rep.* **2018**, 8, 342.
- [72] J. M. Wright, C. A. Merlo, J. B. Reynolds, P. L. Zeitlin, J. G. Garcia, W. B. Guggino, M. P. Boyle, *Am. J. Respir. Cell Mol. Biol.* **2006**, 35, 327.
- [73] E. Hsu, H. Shi, R. M. Jordan, J. Lyons-Weiler, J. M. Pilewski, C. A. Feghali-Bostwick, *Arthritis Rheum.* **2011**, 63, 783.
- [74] M. Selman, G. Carrillo, A. Estrada, M. Mejia, C. Becerril, J. Cisneros, M. Gaxiola, R. Pérez-Padilla, C. Navarro, T. Richards, J. Dauber, *PLoS One* **2007**, 2, e482.
- [75] S. Noguchi, A. Saito, Y. Mikami, H. Urushiyama, M. Horie, H. Matsuzaki, H. Takeshima, K. Makita, N. Miyashita, A. Mitani, T. Jo, *Sci. Rep.* **2017**, 7, 42595.
- [76] S. Esnault, K. Bernau, E. E. Torr, Y. A. Bochkov, N. N. Jarjour, N. Sandbo, *Respir. Res.* **2017**, 18, 188.
- [77] S. Weldon, P. McNally, D. F. McAuley, I. K. Oglesby, C. L. Wohlford-Lenane, J. A. Bartlett, C. J. Scott, N. G. McElvaney, C. M. Greene, P. B. McCray Jr., C. C. Taggart, *Am. J. Respir. Crit. Care Med.* **2014**, 190, 165.
- [78] Y. H. Yang, S. Dudoit, P. Luu, D. M. Lin, V. Peng, J. Ngai, T. P. Speed, *Nucleic Acids Res.* **2002**, 30, 15e.
- [79] R Core Team, *R Foundation for Statistical Computing*, Vienna, Austria.
- [80] L. Gautier, L. Cope, B. M. Bolstad, R. A. Irizarry, *Bioinformatics* **2004**, 20, 307.
- [81] P. Du, W. A. Kibbe, S. M. Lin, *Bioinformatics* **2008**, 24, 1547.
- [82] S. Kaiser, R. Santamaria, T. Khamiakova, M. Sill, R. Theron, L. Quintales, F. Leisch, E. De Troyer, *Biclust: BiCluster Algorithms*, R package, xxx Version 1.2.0, **2013**.
- [83] A. Preli-ç, S. Bleuler, P. Zimmermann, A. Wille, P. Bühlmann, W. Gruissem, L. Hennig, L. Thiele, E. Zitzler, *Bioinformatics* **2006**, 22, 1122.
- [84] R. Tibshirani, T. Hastie, B. Narasimhan, G. Chu, *Proc. Natl. Acad. Sci. U. S. A.* **2002**, 99, 6567.
- [85] T. Hastie, R. Tibshirani, B. Narasimhan, G. Chu, *Pam: Prediction Analysis for Microarrays*, CRAN, 2014-08-27, xxx **2019**.
- [86] M. Husain, D. Wu, A. T. Saber, N. Decan, N. R. Jacobsen, A. Williams, C. L. Yauk, H. Wallin, U. Vogel, S. Halappanavar, *Nanotoxicology* **2015**, 9, 1013.